CIRCULAR SYMMETRY MODELS IN IMAGE PROCESSING

LINKÖPING STUDIES IN SCIENCE AND TECHNOLOGY

Thesis no: 85

Josef Bigün

LIU-TEK-LIC-1986:25
ISSN 0280-7971
ISBN 91-7870-009-X Linköping September 1986

Department of Electrical Engineering
Linköping University
S-581 83 Linköping, Sweden

Linköpings tekniska högskola
Institutionen för Systemteknik
581 83 Linköping

CONTENTS

ACKNOWLEDGEMENT

I would like to express my deepest gratitude to the persons who have contributed to this report in various ways:

To my supervisor, Gösta Granlund, professor of Computer Vision at LiTH. He has been a constant source of inspiration during this work. He has spent a great deal of time on discussions and work to review this manuscript.

To Lars Inge Hedberg, professor of Applied Mathematics at LiTH. He has provided time for valuable discussions when I needed.

To the members of the GOP-group, and in particular, Dr. Hans Knutsson. They have contributed with important comments and ideas for improvements.

To our patient secretary Catharina Holmgren. She has typed parts of the manuscript.

To the Swedish Board for Technical Development which has provided the financial support.

Not least to my brother and sister, Thomas and Helen. They have proved to be indispensable with their sincere encouragement.

Josef Bigün
Linköping University
Department of Electrical Engineering
S-581 83 Linköping
Sweden

ABSTRACT

New methods for feature extraction based on the spectral properties of local neighbourhoods is presented. The spectral behaviour of the neighbourhoods is investigated in the spatial domain using the Parseval relation applied to partial derivative pictures. Two types of such properties are considered for circular symmetric and linear symmetric neighbourhoods. These two properties are the existence of point concentration and line concentration in the spectra. For the circular symmetry investigation a new basis function set is introduced. To obtain a spectrum in the terms of these basis function sets, a scalar product is introduced for circular neighbourhoods. The same is carried out for linear symmetry spectra using the well-known basis set and the scalar product consisting of cosines and $\mathcal{L}^2(\Omega)$ scalar product. Confidence parameters are introduced to measure the significance of the extracted features. These are basically different types of variance measures and they are shown to be specific for the desired information: The existence of point concentration or line concentration in the spectra of the local neighbourhoods.

CHAPTER 1
MODEL BASED FEATURE EXTRACTION

The term feature extraction is widely used in computer vision. It is used in the sense of a neighbourhood dependent mapping of a picture to a function of it. The gray value of every point in the picture resulting from the feature extraction transformation is evaluated from the domain having a closed contour, as boundary in the original picture.

A transformed picture point is associated with a point in the original picture. It is generally a point within the boundary where the transformed picture points originated. We will call this point "the examined point". This is the basis for the concept of neighbourhood dependence referred to earlier. This is what we mean by feature extraction in this paper, which is sometimes referred to as feature detection or even template matching in the literature. It should be mentioned that there exist various views different from ours on what is meant by feature extraction. Moreover we will assume that the closed contour constituting the boundary of the neighbourhood is not changed and is rigid relative to the examined point. The mapping itself characterizes of course, the result. It can be shape detection (two widely known shapes are lines and edges), statistical properties (mean, variance), center of gravity, etc. But we will concentrate on shape detection in the following sections.

The extraction of features is necessary for all aspects of processing and analysis such as classification, segmentation, enhancement and coding. The experience in classification is that if the right features are used then the feature vector will cluster around a particular point for pixels belonging to the same class. The cluster points will be separable in this multidimensional vector space. The distance between the cluster points of different classes is a measure of the goodness of the separation ability of the vector used. Segmentation is a special case of classification in which the classes are natural objects. The features are used in enhancement applications as feedback information to remove noise, while in coding applications they are used as control information [9].

Now to the question of how to extract features connected with special shapes. The answers given are many. Many of the methods are based upon template matchings of the picture using target patterns. However, there are also methods projecting the local neighbourhood onto basis functions connected to target pattern spaces. [10] generalizes this idea to arbitrary shapes through Karhunen-Loewe expansion of the target pattern space. Yet another different method is presented by [5], [6], [8] for orientation and frequency features, based on

frequency plane filters. We will summarize the last two methods and present a third method based on expansion in basis functions, which are not approximating the target pattern space with the least error (in the mean square norm) for a fixed number of basis functions, since they are not the basis functions of the Karhunen-Loewe expansion of target pattern space. But they are dense in a reasonably large space of local neighbourhoods, and thereby approximating the gray values of any neighbourhood arbitrarily well upon increasing the number of approximating basis functions. This is a property which is lacking for the basis functions used in Karhunen-Loewe approach. The reason for this is that the Karhunen-Loewe basis functions only have the property of being dense in the space they are produced (a target pattern space) and not in any larger space (space of all patterns). Moreover the method is not intending to approximate the by neighbourhood by a finite number of basis functions, but the properties of the coefficient spectrum based on an infinite number of basis functions. This is accomplished by the Parseval relation after carefully chosen operations in the neighbourhood. Neither the basis functions nor the chosen operations are intended to have a general derivation form.

The methods, based on finite approximation of the neighbourhoods by basis functions suitable to target patterns, start with a selection of basis functions. This can be formulated mathematically as approximating a target pattern space with a finite number of basis functions such that the approximation error to any target pattern will be small on the average. Indeed this problem formulated as above, is shown to yield a solution which results in a basis set, which minimizes the average approximation error and is not altered dramatically by increasing or decreasing the number of basis functions, other than addition or removal of new bases to the set. This set is the eigen functions of the integral operator having the auto correlation function of target patterns as kernel and can be found in most textbooks in statistics, (The Karhunen-Loewe expansion of random processes). Denote the target pattern space by S and assume that the index $\bar{p}$, a finite dimensional real vector that exhausts S, then the eigenvalue problem is:

$$\int_{\bar{r}' \in \Omega} R(\bar{r}, \bar{r}') \phi_i(\bar{r}') d\Omega = \lambda_i \phi_i(\bar{r})$$

Where $R(\bar{r}, \bar{r}')$ is $E[x_{\bar{p}}(\bar{r}) x_{\bar{p}}(\bar{r}')]$ with $x_{\bar{p}}$ being a target pattern which is considered as a stochastic function with suitable probability distribution of $\bar{p}$ over the event space. The event space is of course the target pattern space S. Ω is the neighbourhood in which the examined point lies. The infinite and complete basis set consists of the eigen functions $\{\phi_i\}$,

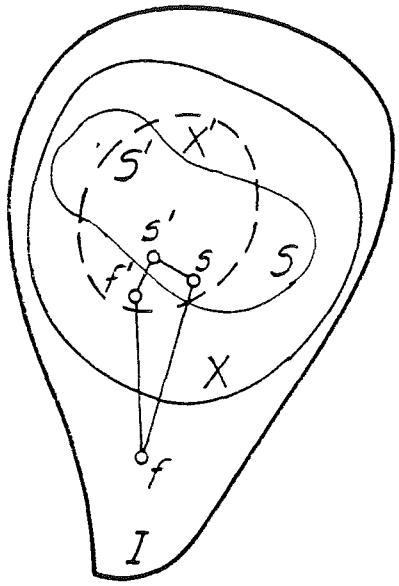

Figure 1.1) The figure illustrates the function spaces referred in [10].

which are orthogonal in the usual $\mathcal{L}^2(\Omega)$ sense:

$$(f,g) = \int_{\Omega} f^*(\bar{r})g(\bar{r})d\Omega$$

Denote the space which can be linearly spanned by $\{\phi_i\}$ as X.

All eigen values, λ_i are positive since the kernel is an autocorrelation function and thereby it forms a positive definite compact integral operator, [4]. The required finite set with the least errors consists of eigen functions belonging to the largest eigen values and we will denote it by X'. The algorithm can be visualized as in Figure 1.1) and carried out as in the following steps:

Let I be the set of all patterns which can occur in the given neighbourhood.

1) Project I to X'; that is for a target pattern f in I find an f' in X' by calculating the coefficients c_m in the relationship:

$$f' = \sum_{m=1}^{M} c_m \phi_m$$

as

$$c_m = (f, \phi_m) = \int_\Omega f(\bar{r})\phi_m(\bar{r})d\Omega$$

2) Let S' be the projection of target pattern space S to the space spanned up linearly by the finite basis space, X'. Then find an element s' in S' such that $\|s' - f'\|$ is minimized over S'. The norm is $\mathcal{L}^2(\Omega)$ norm to utilize the advantages of the inner product space. [10] suggests to use $\|s' - f'\|$ as confidence parameter when it is large because of the inequality,

$$\|s' - f'\| \leq \|s - f\|$$

in which s is the member of S which minimizes the distance $\|s - f\|$,

The s' found in step 2) is then close to the ideal one, s, if f is a pattern close to a target pattern.

The approach is general but not possible to perform in practice easily because:

1) Except in very special cases, explicit solutions to the integral eigenvalue problem are difficult to obtain. The problem, somehow, should then be approximated by a discrete one and solved numerically.

2) Minimization of $\|s' - f'\|$ is often nontrivial and too cumbersome to be performed for a large amount of examined points in the picture. To be performed, the method is highly dependent on low dimensionality of X', if at all possible to pursue.

However, the above difficulties are passed by successfully for the orientation detection problem of edges and can be found in [10]. But great care and a large portion of chance is required to pass by 1) and 2) to successfully carry out the algorithm for feature detection of general target patterns. Alternatively the finite basis functions are chosen intuitively instead of Karhunen-Loewe expansion of target patterns to find explicit or easily implemented implicit solutions to the minimization of $\|s' - f'\|$.

In another method, [8] solves the problem of finding orientation in real pictures by a different approach. One starts by assuming that the local neighbourhood is a part of a planar wave. Then one looks at the filter outputs of a number of quadrature filters. The answers from the

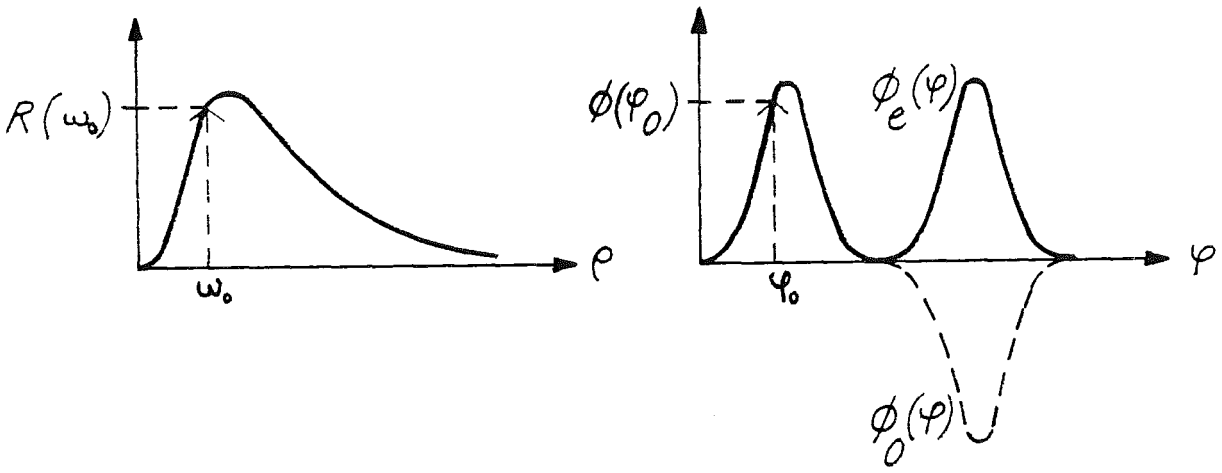

Figure 1.2) The filters used in [5], [8] are separable in polar coordinates. The figure illustrates the radial and angular parts of these together with the response of a pure sinusoid as input.

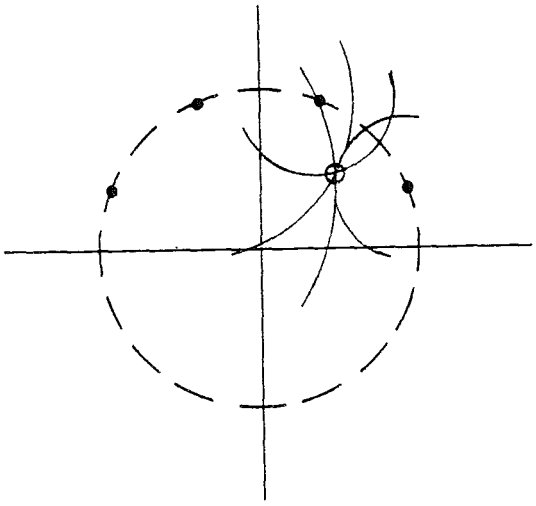

Figure 1.3) The figure illustrating the problem of finding the location of the sinusoid spikes in the fourier plane which is viewed from the top.

filters are thus the amplitudes of frequency responses of the filters, at the frequency vector of the planar wave.

The problem is then reduced to finding the location of the spikes from the filters.

This problem can be shown to be solved easily by a linear combination of the amplitudes of the filter responses. The argument of the resulting complex number is the orientation of the wave, $2\varphi_0$. Finding ω_0 implies similar simplicity, involving a few sets (2 or 3) of filters, with different center frequencies. The point is that when the signals within neighbourhoods are not pure planar waves, for which we neither can nor will see an orientation (or frequency), the magnitude of the resulting complex number, obtained by a complex weighting of filter response magnitudes, decreases if the energy of the neighbourhood is not clustering in the frequency domain. By representing the obtained orientation vectors such that the magnitude corresponds to intensity and the argument to color of a TV monitor, one gets dark areas where the existence of a particular orientation in the vicinity of the examined point is not obvious. Where it is obvious one can see colored lines and edges since the geometry of nature is continuous.

The main difference of the approaches described above for extracting orientation information is that the first one is a spatial domain method while the latter is a frequency domain method. The first one is more general in the sense that other features than orientation of edges can be handled. But in practice this generality often has a very high price. This is due to the fact that the minimization process of $\|s' - f'\|$ over the set S', referred to above, is a non trivial task, if convergence ever exists. In both methods the evaluation of features is done entirely in the spatial domain.

In the following we will introduce a new approach to certain types of vparameter extraction problems defined by a model. And in the following chapters we will give two such models: Circular symmetry and linear symmetry models. The purpose will be to find circular symmetry parameters and linear symmetry parameters if the vicinity of the examined point has such a property. The approach has a touch of both methods summarized above.

The critical but not always fulfilled assumption is that there exists a Hilbert space X, with the orthonormal function set $\{\phi_m\}$ spanning X, which is dense in the local neighbourhood space I, and fulfills either of the following:

1) The feature to be extracted should be the basis functions ϕ_m that is the existence of ϕ_m or a scalar times it in the neighbourhood. However, this is a severe restriction, since the feature desired, or more correctly the functions through which the features are defined, may not constitute an orthonormal dense Hilbert space in the neighbourhood space, I, considered. As an example, ideal step edges in the usual $\mathcal{L}^2(\Omega)$ scalar product with Ω being a rectangle

do not fulfill this requirement.

2) The feature to be extracted is a property of the functions ϕ_m. For example orientation of edges in the neighbourhood can be connected to $\{e^{i\bar{k}.\bar{r}}\}_{\bar{k}}$ where the vector $\bar{k}$ is chosen to be $(m\frac{2\pi}{L_x}, n\frac{2\pi}{L_y})$ with integers m, n and rectangle side lengths L_x and L_y respectively.

Often in computer vision context it is not the existence of a robust template in the neighbourhood which is interesting, but the properties of it. In our approach this will be equivalent to investigate certain types of behavior in the coefficient plane. For example in the case of lines/edges one can talk about a definitive direction of the line in the neighbourhood. By investigating whether there exists an energy concentration along a specific direction, one should be able to find the direction of the line. We will call this property line concentration, since the portrait of lines and edges is characterized by a concentration of energy along a line in the Fourier plane. Another type of behaviour of the energy distribution is a concentration around a point in the coefficient plane. Experiments, [8], show that this type of concentration corresponds to regularity in the textures, which coincides with our intuition, since a pure point concentration of the energy to a specific point means existence of a sinusoid in the neighbourhood. In the following chapters we will only consider these two types of energy distribution. We will in the following give a summary of the feature extraction for point concentrations. The line concentration investigation is quite similar.

Since perfect point concentration defines a pure sinusoid we will associate one of the functions $\{\phi_m\}$ to the neighbourhood and give a confidence parameter to the the success of this association in the following manner: By relating a ϕ_m which has the property of having a definite direction, through $\bar{k}$, that is parallel lines as iso-gray values of ϕ_m, one should be able to define the local orientation of the neighbourhood. Furthermore if the feature to be extracted is a characteristic and inevitable property of the template by which it is defined, then it is possible to decide whether the neighbourhood matches the template. This can be done by deriving some type of confidence parameter starting the success of the assignment of ϕ_m to the neighbourhood. The proposed approach for feature extraction for point concentration can thus be summarized as below:

1. Association of a $\phi_{m'}$ function to the neighbourhood, f, by expansion of the neighbourhood in ϕ_m and choosing a $\phi_{m'}$ based on the coefficient configuration.

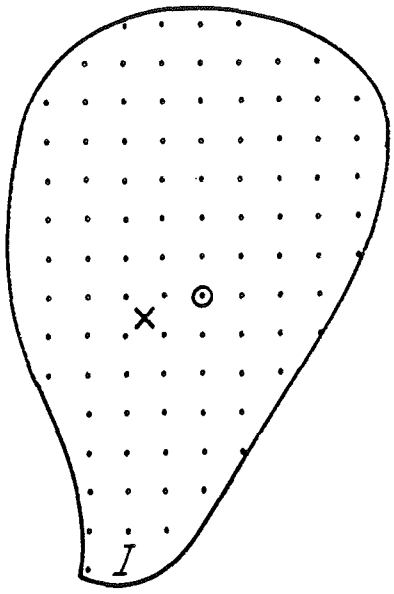

Figure 1.4) The proposed approach for feature extraction for point concentration considers an ON-base which spans all neighbourhoods. The cross illustrates the approximation of the position of the dominating basis function. The encircled point illustrates the position of the largest energy.

$$f = \sum_{m \in Z} c_m \phi_m \qquad \text{where} \quad Z = \{0, \pm 1, \pm 2 ...\}$$

The choice should be made in such a way that if there is just one term in the expansion such that the neighbourhood matches to one of the basis functions, then the choice is the correct one, (projection property). In other cases the choice should be close to the dominating term or the term which has the largest energy, $|c_m|^2$. In the circular and linear symmetry cases it is proposed to be a type of mean value.

2. Association of a confidence parameter to the projection parameter explained in 1). The confidence parameter should assume large values when the feature exists in the neighbourhood. This existence may be modelled to be equivalent to the existence of unimodality in the spectrum of f.

Here we are confronted by the very fact that we are trying to describe the shape of spectral density which has obviously the degree of infinity by a single parameter $C_{\Omega m}$ or $C_{\Omega n}$ We can, however, not hope to find a functional which manages this. What we can find is a functional which tells us whether the neighbourhood frees some prescribed hypothesis. In this case we

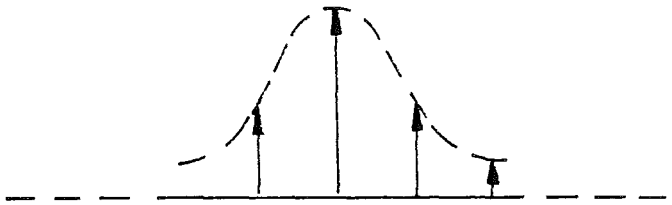

Figure 1.5) A point concentration has the property of unimodality. The basis functions with the largest energies are situated close to each other in the coefficient plane.

will require that:

a) it should be unique when match occurs

b) it should respond monotonically when the degree of mismatch, measured in some manner, increases.

CHAPTER 2
CIRCULAR SYMMETRY MODELING

There is a long list of operators that detect the existence of linear symmetry in a local neighbourhood. Most of them measure linear symmetry in the sense of lines and edges. But there is very little done to model circular symmetry. This is perhaps so because pictures of objects in nature are usually more irregular than circles. Nevertheless we believe that it is one of the symmetries which human beings utilize in early vision and we think that circular symmetry should be a complementary symmetry model to the linear symmetry model which has been exposed to extensive investigations in terms of line and edge detection in the last decades. The fact that circularly symmetric shapes like rotating fans, diverging rays, circularly propagating water waves... e.t.c. are observed as phosphenes when low frequency magnetic fields are applied to the temples, [1], [2], does not make this belief less probable. Moreover many manufactured objects are locally concentrated and have closed roundish boundaries. Many natural objects in low resolution pictures exhibit this property like cells seen under microscope. Thinkable application areas are object counting, classification and image coding and enhancement for certain types of pictures, possessing local circular symmetry properties. In this chapter we will model circular symmetry keeping in mind the guiding principles we proposed in the previous chapter for extraction of template based features. But first we should have a more precise statement about what kinds of patterns are called circularly symmetric in our terminology since it is quite a vague concept otherwise.

DEFINITION: We will call local neighbourhoods circularly symmetric if the locus of iso-gray values constitute parallel lines in polar coordinates:

$$k_1 r + k_2 \varphi + k_3 = 0 \qquad r \geq 0$$

with some constants k_1, k_2, and k_3. We will assume that the neighbourhood's boundary is a circle and origin is the center of this circle.

DEFINITION: $C^2(\Omega)$ is the space of complex valued functions which have continuous second derivatives in Ω. Ω is a circle with radius R except the origin.

$$\Omega = \{|\bar{r}| \leq R\} \backslash \{\bar{0}\}.$$

DEFINITION: (f, g) is the scalar product for functions $f, g \in C^2(\Omega)$ with

$$(f,g) \stackrel{\triangle}{=} \frac{1}{|\Omega|} \int_\Omega \frac{1}{r} f^*(\bar{r}) g(\bar{r}) d\Omega$$

with $r = |\bar{r}|$ and:

$$|\Omega| = \int_{\Omega} \frac{1}{r} d\Omega.$$

That this definition fulfills the scalar product axioms can be checked readily

1) $(f, g) = \overline{(g, f)}$ for all $f, g \in C^2(\Omega)$

2) $(h, \alpha f + \beta g) = \alpha(h, f) + \beta(h, g)$ for all $f, g, h \in C^2(\Omega)$

3) $(f, f) > 0$; $(f, f) = 0$ if and only if $f = \bar{0}$.

Consider the functions

$$\Psi_{mn}(\bar{r}) = e^{i(m\omega r + n\varphi)} \tag{1}$$

with $w = \frac{2\pi}{R}$ and $m, n \in Z$. The completition of $C^2(\Omega)$ is a Hilbert space with the following scalar product

$$\frac{1}{2\pi R} \int_0^{2\pi} \int_0^R \bar{f}(r, \varphi) g(r, \varphi) dr d\varphi$$

Moreover $\{\Psi_{mn}\}_{m,n \in Z}$ is dense in $C^2(\Omega)$, which follows from the Fourier series expansion theory on a rectangle, [3]. But this scalar product is the same scalar product defined earlier with, Ω, being a circle. By that we can use the fourier series expansion theory of functions on a circle, as if we dealed with the usual expansion in sines and cosines on a rectangle. Now let us consider the neighbourhood Ω, around an examined point in a picture. Assume that the polar coordinates, $r = |\bar{r}|$ and $\varphi = arg(\bar{r})$, referred in the following are relative to the examined point, and the horizontal positive half line from the examined point, Figure 2.1).

Let the real function $f(\bar{r})$ express the gray values in Ω, placed around the examined point, such that $\bar{r}$ is the local coordinate vector. Then one can expand f as

$$f(\bar{r}) = \sum_{m,n \in Z} c_{mn} \Psi_{mn}(\bar{r}) \tag{2}$$

with

$$\begin{aligned} c_{mn} &= (f, \Psi_{mn}) \\ &= \frac{1}{2\pi R} \int_{\Omega} \frac{1}{r} f(\bar{r}) e^{i(m\omega r + n\varphi)} d\Omega \end{aligned} \tag{3}$$

because the completition of $C^2(\Omega)$ is a Hilbert space and $\{\Psi_{mn}\}_{m,n \in Z}$ constitute a complete

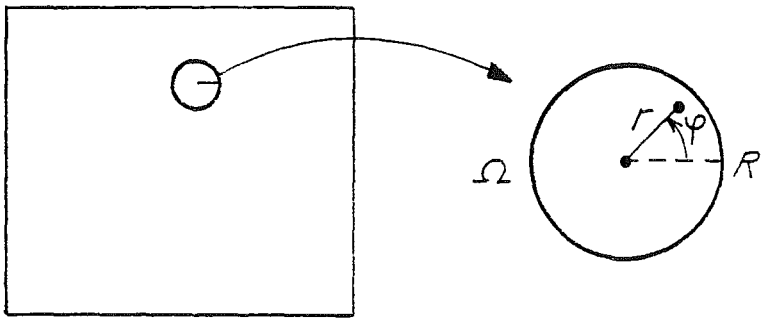

Figure 2.1) The figure illustrates the domain, Ω, in which the gray value function $f(\bar{r})$ is defined. $\bar{r}$ is coordinate vector relative to the examined point. Above, the polar version of $\bar{r}$ is indicated.

orthonormal base in that space:

$$\begin{aligned}(1, \Psi_{mn}) &= \frac{1}{2\pi R} \int_{\Omega} \frac{1}{r} e^{i(m\omega r + n\varphi)} d\Omega \\ &= \frac{1}{2\pi R} \int_0^{2\pi} \int_0^R e^{i(m\omega r + n\varphi)} dr\, d\varphi \\ &= \delta_{m0}\delta_{n0}\end{aligned}$$

and hence

$$(\Psi_{mn}, \Psi_{m'n'}) = \delta_{mm'}\delta_{nn'} \tag{4}$$

$\delta_{mm'}$ is the kronecker delta with the usual definition:

$$\delta_{mm'} = \begin{cases} 1, & \text{if } m = m'; \\ 0, & \text{otherwise.} \end{cases}$$

LOCAL NEIGHBOURHOOD MODELLING

We are going to model the local neighbourhood by means of a modified version of the expansion given in (2) and (3). It is simply an even expansion in the local radial coordinate, r of the neighbourhood.The reason for this is that we want to express real neighbourhoods in terms of real templates given by $\Psi_{mn} + \Psi_{-m-n}$, which are easy to visualize and to interpret.

We wish to find some sort of mean value over all (n, m) tuples (countable but infinite in number) weighted by their energy contribution to the total energy. By means of these mean values, which we will present in the following parts of this chapter, we will infere whether there exist circular symmetry property in the neighbourhood. For real pictures f, assuming the expansion given by (2) and (3):

$$\begin{aligned} c_{mn} =& \frac{1}{|\Omega|}\int_{\Omega}\frac{1}{r}f(\bar{r})\Psi_{mn}(\bar{r})d\Omega \\ =& \frac{1}{2\pi R}\int_0^{2\pi}\int_0^R f(r,\varphi)cos(m\omega r + n\varphi)drd\varphi \\ &+ \frac{i}{2\pi R}\int_0^{2\pi}\int_0^R f(r,\varphi)sin(m\omega r + n\varphi)drd\varphi \\ =& \frac{1}{2\pi R}\int_0^{2\pi}\int_0^R f(r,\varphi)cos - (m\omega r - n\varphi)drd\varphi \\ &- \frac{i}{2\pi R}\int_0^{2\pi}\int_0^R f(r,\varphi)sin(-m\omega r - n\varphi)drd\varphi \\ =& \bar{c}_{-m-n} \end{aligned} \tag{5}$$

which is the hermitian property of the coefficients. Thus (5) gives

$$|c_{mn}| = |c_{-m-n}|$$

This means that an energy profile through origin in the coefficient plane is even and may look like in figure 2.2)

and the mean values for m and n vanish for all real neighbourhoods. Because

$$\sum_{m,n\in Z} mc_{mn}^2 = 0$$

$$\sum_{m,n\in Z} nc_{mn}^2 = 0$$

That is we can not get any information about which coefficient is dominating in the expansion by a straight forward mean value evaluation, due to the symmetry in the coefficient plane. In other words, we should carry out mean value evaluation in a half plane, figure 2.5).

Before we propose some measures revealing the behavior of coefficients let us expand the local neighbourhood in an even manner. The only reason for this is technical as mentioned earlier. This implies that Ω defined as above should be changed to a somewhat more abstract one to comprise negative values of r as well.

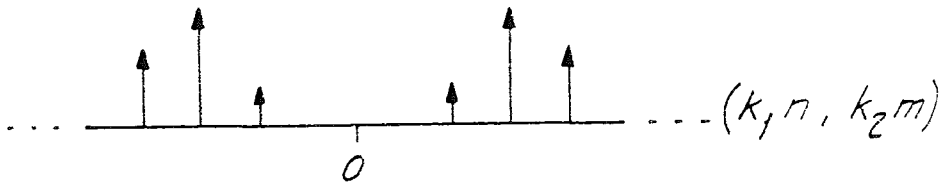

Figure 2.2) $k_1 n + k_2 m = 0$ axis in the coefficient plane for some integers k_1 and k_2. m or n is swept through $0, \pm 1, \pm 2...$

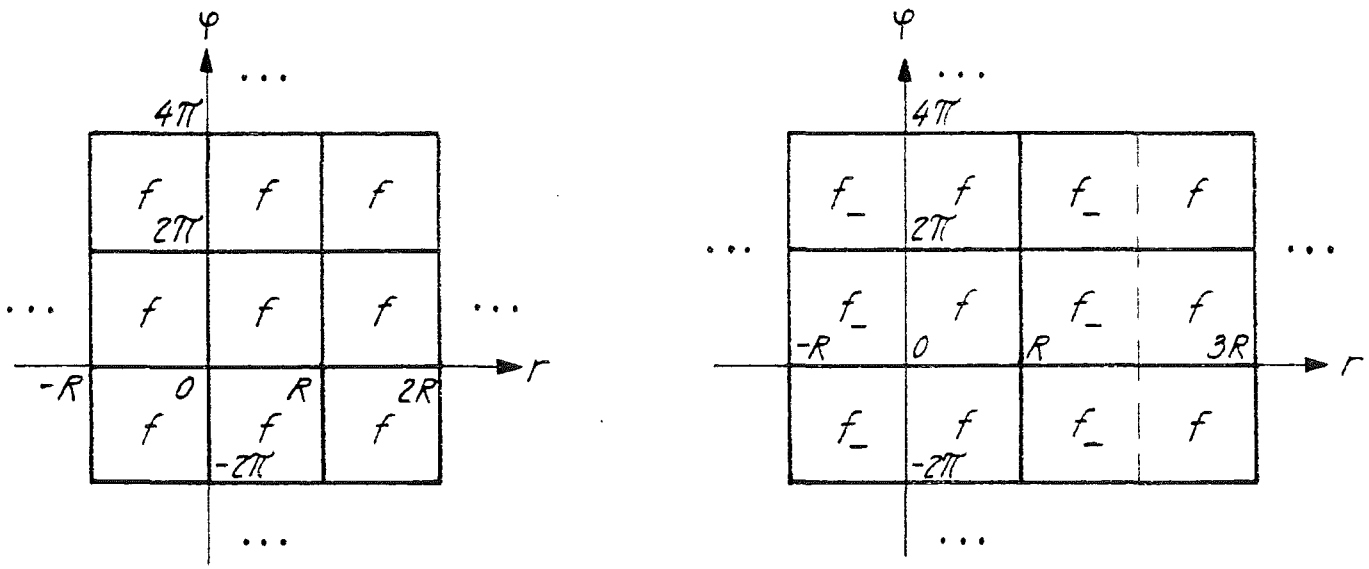

Figure 2.3) Function f is originally defined on $[0, R] \otimes [0, 2\pi]$ and naturally periodized in φ direction with period 2π, figure to the left, we extend f's definition domain to comprise even negative values of r. The basic rectangle becomes $[-R, R] \otimes [0, 2\pi]$, figure to the right. f_- is defined through $f(-r, -\varphi) = f(r, \varphi)$. In both illustrations basic rectangles are marked by bold lines.

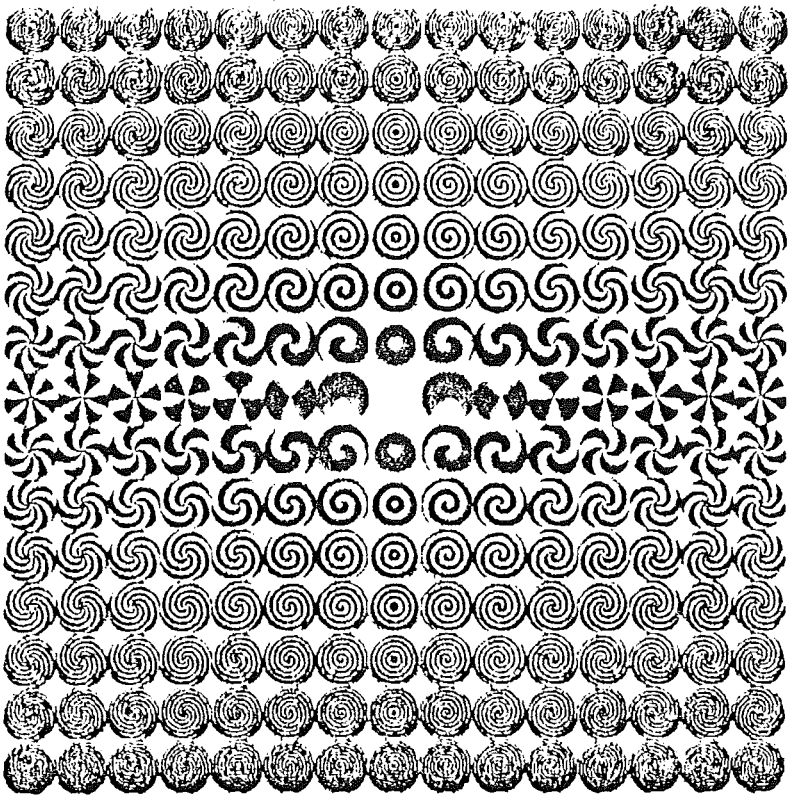

Figure 2.4) Figure shows a sampled version of ϕ_{mn} with $R = 15$ and different m, n. The parameters m and n are orders for the frequencies of sinusoid waves in radial and angular directions respectively.

It is thus:

$$\Omega = \{(r,\varphi) \in \mathcal{R}^2 : \qquad r \in [-R,R] \quad , \quad \varphi \in [0,2\pi]\}$$

and the image is defined on those parts of Ω which were not defined, as:

$$f(-r,-\varphi) = f(r,\varphi) \qquad (r,\varphi) \in [0,R] \otimes [0,2\pi]$$

by doing this we do not, of course, affect the behavior of f in $[0,R] \otimes [0,2\pi]$ since this is a subset of Ω and f is the same in this subset as before. Hence

$$f(r,\varphi) = \sum_{m,n \in Z} c_{mn} \Psi_{mn} \tag{6}$$

with an ON-basis function set differing slightly in ω compared to (1):

$$\Psi_{mn} = e^{i(m\omega r + n\varphi)} \qquad \text{where} \qquad \omega = \frac{\pi}{R}$$

like $|\Omega|$ and c_{mn} which are $4\pi R$ respectively (f, Ψ_{mn})

with the scalar product defined as:

$$(f,g) = \frac{1}{4\pi R} \int_0^{2\pi} \int_{-R}^{R} \bar{f}(r,\varphi) g(r,\varphi) dr d\varphi$$

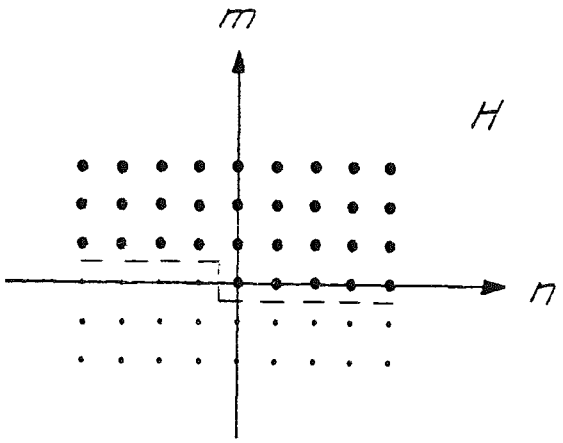

Figure 2.5) Figure showing, the members of H which is the subset of Z, consisting of all points in the (n, m) plane.

Then c_{mn} will be real and even

$$\begin{aligned} c_{mn} =& \frac{1}{4\pi R}\int_0^{2\pi}\int_{-R}^{R} f(r,\varphi)cos(m\omega r + n\varphi)drd\varphi \\ &+ \frac{i}{4\pi R}\int_0^{2\pi}\int_{-R}^{R} f(r,\varphi)sin(m\omega r + n\varphi)drd\varphi \\ =& \frac{1}{4\pi R}\int_0^{2\pi}\int_{0}^{2R} f(r,\varphi)cos(m\omega r + n\varphi)drd\varphi \end{aligned} \tag{7}$$

since f is even . (6) establishes also

$$f = \sum_{m,n\in H} c_{mn}(\Psi_{mn} + \Psi_{-m-n}) - c_{00}$$

with

$$H = \{m,n: \qquad \{m,n: \quad m \geq 0\}\backslash\{m,n: \quad m = 0, n < 0\}\}$$

since $c_{mn} = c_{-m-n}$.

Thus

$$f = \sum_{m,n\in H} a_{mn}\phi_{mn} \tag{8}$$

can be written with ϕ_{mn} being:

$$\phi_{mn} = \frac{cos(m\omega r + n\varphi)}{\|cos(m\omega r + n\varphi)\|}$$

also ϕ_{mn} defined above with $(n,m) \in H$ constitute an ON base for functions which are periodic, with periods $2R$ and 2π in the radial and angular directions. To see this let us construct:

$$
\begin{aligned}
&(\phi_{mn}, \phi_{m'n'}) = \\
&\frac{(\Psi_{mn}, \Psi_{m'n'}) + (\Psi_{mn}, \Psi_{-m'-n'}) + (\Psi_{-m-n}, \Psi_{m'n'}) + (\Psi_{-m-n}, \Psi_{-m'-n'})}{\|\Psi_{mn} + \Psi_{-m-n}\| \|\Psi_{m'n'} + \Psi_{-m'-n'}\|} \\
&= \frac{\delta_{mm'}\delta_{nn'} + \delta_{m-m'}\delta_{n-n'} + \delta_{-mm'}\delta_{-nn'} + \delta_{-m-m'}\delta_{-n-n'}}{\sqrt{(\delta_{m-m}\delta_{n-n} + \delta_{-mm}\delta_{-nn} + 2)(\delta_{m'-m'}\delta_{n'-n'} + \delta_{-m'm'}\delta_{-n'n'} + 2)}} \\
&= \frac{\delta_{mm'}\delta_{nn'} + \delta_{m-m'}\delta_{n-n'}}{\sqrt{(\delta_{m-m}\delta_{n-n} + 1)(\delta_{m'-m'}\delta_{n'-n'} + 1)}}
\end{aligned}
$$

since the kronecker delta is an even function. Only the following three cases occur for (n,m) and $(n',m') \in H$:

a) $m \neq 0$

$$(\phi_{mn}, \phi_{m'n'}) = \frac{\delta_{mm'}\delta_{nn'}}{\sqrt{\delta_{m'-m'n'-n'+1}}} = \delta_{mm'}\delta_{nn'}$$

b) $m = 0 \quad n \neq 0$

$$
\begin{aligned}
(\phi_{0n}, \phi_{m'n'}) &= \frac{\delta_{0m'}\delta_{nn'} + \delta_{0-m'}\delta_{n-n'}}{\sqrt{(\delta_{00}\delta_{n-n} + 1)(\delta_{m'-m'}\delta_{n'-n'} + 1)}} \\
&= \frac{\delta_{0m'}\delta_{nn'}}{\sqrt{\delta_{m'-m'}\delta_{n'-n'} + 1}} = \delta_{0m'}\delta_{nn'}
\end{aligned}
$$

because $\delta_{n-n'} = 0$ for $(n,m), (n',m') \in H$.

c) $m = 0 \quad n = 0$

$$
\begin{aligned}
(\phi_{00}, \phi_{m'n'}) &= \frac{\delta_{0m'}\delta_{0n'} + \delta_{0-m'}\delta_{0-n'}}{\sqrt{(\delta_{00}\delta_{00} + 1)(\delta_{m'-m'}\delta_{n'-n'} + 1)}} \\
&= \frac{2\delta_{0m'}\delta_{0n'}}{\sqrt{2(\delta_{m'-m'}\delta_{n'-n'} + 1)}} = \delta_{0m'}\delta_{0n'}
\end{aligned}
$$

Hence

$$(\phi_{mn}, \phi_{m'n'}) = \delta_{mm'}\delta_{nn'} \tag{9}$$

Thus a_{mn} will be

$$a_{mn} = (f, \phi_{mn}) = \sqrt{2}\frac{c_{mn}}{\sqrt{(\delta_{m-m}\delta_{n-n} + 1)}} \tag{10}$$

since (6) is valid so is (8):

$$\lim_{M,N_1,N_2\to\infty} \|f(r,\varphi) - \sum_{n=-N_1}^{N_2}\sum_{m=0}^{M} a_{mn}\phi_{mn}\| = 0$$

for $(r, \varphi) \in [0, R] \otimes [0, 2\pi]$.

POINT CONCENTRATION SEEN AS PPROJECTION TO A COUNTABLE SET $\{\phi_{mn}\}$

DEFINITION: Let P be an operator from $C^2(\Omega)$ to the function set X, $X \subset C^2(\Omega)$. Then P is a projection from $C^2(\Omega)$ to X if

$$P^2 f = Pf$$

for all f in $C^2(\Omega)$.

Our goal is to find an algorithm based on operations done in the spatial domain but still giving us some understanding about whether the energy is concentated to a point in the frequency domain. The algorithm should posses the following properties:

1) Whenever the neighbourhood, $f(\bar{r})$, consists of just one of the basis functions, ϕ_{mn}, except possibly an amplifiying scalar A, the algorithm should detect this particular basis function. That is $(f, \phi_{m'n'}) = 0$ except for the tuple (n, m). In other cases it should give some sort of dominating tuple (n,m). Given the tuple (n, m), ϕ_{mn} is unique. Call the operator of finding (n, m), and associating the function ϕ_{mn} to that, as P then:

$$P^2 f = Pf = \phi_{mn}$$

for any $f \in C^2(\Omega)$. This is equivalent to saying that the sought algorithm is a projection to the countable set $\{\phi_{mn}\}$, according to the definition above.

2) The projection parameter should be rotation and radial phase invariant for pure inputs of:

$$f(r, \varphi) = A\phi_{mn}(r, \varphi)$$

with some scalar A. That is

$$Pf(r + r_0, \varphi + \varphi_0) = Pf(r, \varphi) = \phi_{mn}$$

fullfilled.

3) Whenever the local neighbourhood differs from a circular symmetric pattern a confidence parameter should reflect that. By attaining high values, for example, this parameter could be used to highlight the relevance of the projection parameter, and conversely to suppress it if the neighbourhood differs from a circular symmetric pattern.

The use of confidence parameters is due to [5]. One combines the confidence parameter and projection parameter together in every point of the picture to form a vector, in such a way that the magnitude of this vector becomes confidence parameter and argument of it becomes projection parameter. The magnitude can then be allowed to modulate the intensity of a point in a color TV monitor and the argument of it, representing the projection parameter, to modulate the color of same point. The result is a color picture representing a decision in every neighbourhood of the original picture. The projection parameter and the confidence parameter values evaluated in every point in the picture can be thought to be as two separate pictures influencing each other. A point with low confidence level in the resulting picture looks dark no matter what the color of the point or the projection parameter.A point with high confidence level is illuminated to reveal it's color.

The algorithm consists of doing the computations described by (11)-(15) and finding:

a) a dominating radial frequency measure, $\hat{m}$ and an associated confidence measure, $C_{\Omega m}$, which is the degree of match between the model and the neighbourhood.

b) a dominating angular frequency measure, $\hat{n}$ with it's associated confidence measure $C_{\Omega n}$.

$$A \triangleq \|f\| \tag{11}$$

$$m_d \triangleq \frac{\|D_r f\|}{A\omega} \tag{12}$$

$$n_d \triangleq \frac{\|D_\varphi f\|}{A} \tag{13}$$

$$C^2_{\Omega m} \triangleq \frac{\|D^2_r f\|^2}{A^2\omega^4} - m_d^4 \tag{14}$$

$$C^2_{\Omega n} \triangleq \frac{\|D^2_\varphi f\|^2}{A^2} - n_d^4 \tag{15}$$

There are some difficulties with directly assigning m_d and n_d to $\hat{m}$ and $\hat{n}$, since all the members of the projection set, $\{\phi_{mn}\}$, have integer valued m and n. Moreover, n can take positive as well as negative integer values. We will simply assign to $\hat{m}$ and $\hat{n}$ the closest integer to m_d and n_d with proper sign:

$$\begin{aligned} \hat{m} &= round(m_d) \\ \hat{n} &= sign \times round(n_d) \qquad sign \in \{-1, 1\} \end{aligned} \tag{16}$$

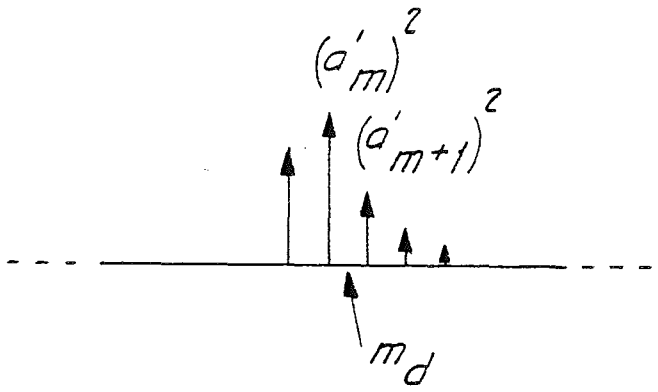

Figure 2.6) Radial frequency is thought of as being the sum of all angular energy contributions at a given frequency m: ${a'_m}^2 = \sum_n a^2_{mn}$ for $(n,m) \in H$. Then m_d should point out a location close to the largest radial frequency component.

It will later be shown that the decision of sign, which determines whether the spirals are twisted clockwise or counterclockwise, does not affect an extra computation other than a comparison.

Let us see what (11)-(15) does to a neighbourhood :

$$f = \sum_{m,n \in H} a_{mn} \phi_{mn} \tag{17}$$

We get through (11)

$$A^2 = \sum_{m,n \in H} a^2_{mn}$$

That is the energy of the neighbourhood in terms of the circularly symmetric function ϕ_{mn} (8)-(10) together with (17) yields:

$$\begin{aligned} m_d = \frac{\|D_r f\|}{A\omega} &= \| \sum_{m,n \in Z} i \frac{m c_{mn}}{A} \Psi_{mn} \| \\ &= \Big(\sum_{m,n \in Z} \frac{c^2_{mn}}{A^2} m^2 \Big)^{\frac{1}{2}} = \Big(\sum_{m,n \in H} \frac{a^2_{mn}}{A^2} m^2 \Big)^{\frac{1}{2}} \end{aligned} \tag{18}$$

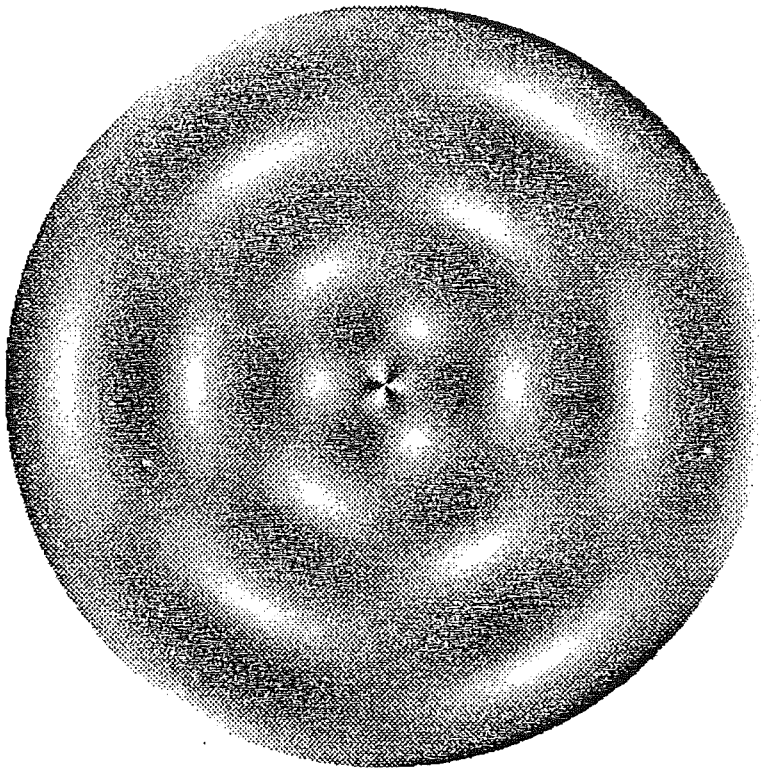

Figure 2.7) Picture of a $\phi_{mn} + \phi_{-m-n}$ neighbourhood

Hence m_d is the weighted root mean square of all radial frequency measures, m. It should be obOBserved that a particular radial frequency number, m, is weighted by the uniform sum of all angular frequency energies, figure 2.6). The weights constitute the energy distribution of the input function. The higher the energy share of ϕ_{mn}, that is $\frac{a_{mn}^2}{A^2}$, the more m_d will be to the favor of m. (18) fulfills obviously the projection requirement after rounding m_d to the closest integer, $\hat{m}$. Similarly, n_d will be the weighted mean square of all orders of angular frequency:

$$n_d = \Big(\sum_{m,n \in H} \frac{a_{mn}^2}{A^2} n^2 \Big)^{\frac{1}{2}} \tag{19}$$

The latter is insensitive to the sign changes in n. A "left twin", say with the order n, is equally treated with a right twin", with the order -n. The consequence of this is a neighbourhood of $f = \phi_{mn} + \phi_{-m-n}$, figure 2.7), is decided to be a $\phi_{m|n|}$ input. The decision is to the favor of one of the equally strong candidates, while an alternative weighting taking the twisting direction into account would see ϕ_{mn} and ϕ_{m-n} as competitors and deliver the answer ϕ_{m0}. Even this would satisfy the projection demand, earlier. However it is more difficult to realize. When $f = \phi_{mn}$ then $m_d = m$ and $n_d = |n|$ which in turn reflects the necessity of the variable *sign* referred earlier (16). We will come back to decision of the *sign* later.

Confidence parameter $C_{\Omega m}$ is proposed to be as in (14), and yields through (8), (10), (18)

$$C_{\Omega m}^2 = \frac{\|D_r^2 f\|^2}{A^2\omega^4} - m_d^4 = \sum_{m,n\in H} \frac{a_{mn}^2}{A^2} m^4 - \sum_{m,n\in H} \frac{a_{mn}^2}{A^2} m^2 m_d^2$$

$$= \sum_{m,n\in H} \frac{a_{mn}^2}{A^2} (m^2 - m_d^2)^2$$

which can be viewed as a weighted variance for the integers m^2. $C_{\Omega n}$ yields a similar expression. The confidence parameter attains it's minimum at the case when

$$\frac{a_{mn}^2}{A^2}(m^2 - m_d^2)^2 = 0$$

for all $(n, m) \in H$. This occurs if and only if

$$\sum_n \frac{a_{mn}^2}{A^2} = 1$$

for some $m = m'$. Thus if $C_{\Omega m}$ is zero then there exists one unique radial frequency in the neighbourhood. And it is given by the estimation, m_d. Since $C_{\Omega m}$ is a variance it also reveals some information about the shape of spectral density, figure 1.5), of the neighbourhood. If $C_{\Omega m}$ is small then it is likely to think that the neighbourhood is a degraded version of a wave with a well defined radial frequency, m_d. Conversely it is unlikely to think that the neighbourhood will have an interpretation, in the term of delivered radial frequency m_d, if $C_{\Omega m}$ is large.

Thus far we have dealed with spectrum concentration around a point. We have obtained parameter estimations of the neighbourhood in terms of a model and found confidence measures for these estimations, working as reliable (in the sense that they were unique when match existed) match detectors. However one can be tempted to find out if it is possible to detect other types of energy concentrations in the coefficient space. In other words: is it possible to find confidence measures for clustering in a given pattern, like we found for clustering around a point? If the answer is yes, can we be certain about the uniqueness of the indication? The answer is yes, for many patterns. Let us investigate clustering of the energy to a line. It is an important case because it corresponds to orientation detection in spatial domain.

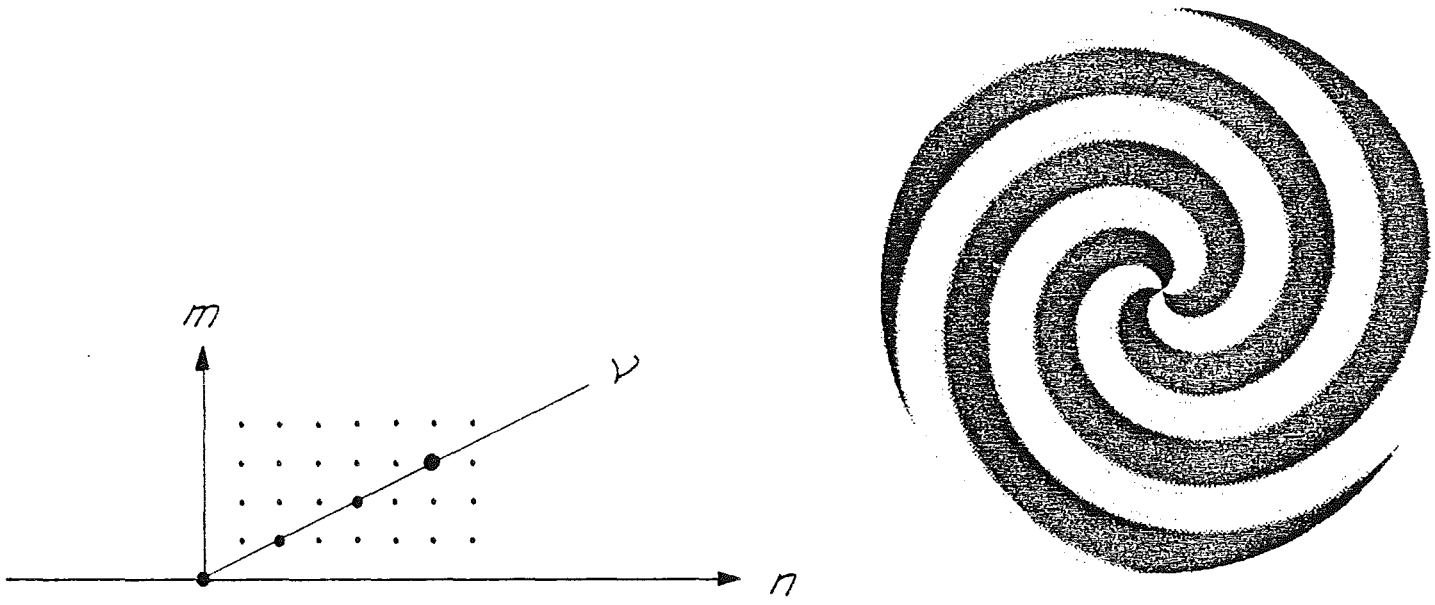

Figure 2.8) Figures showing a coefficient domain and spatial domain pair, with line concentration in the coefficient domain. ν is the length measure in the lines direction.

LINE CONCENTRATION OF ENERGY

Let the line we look for be

$$n = \cot(\theta)m \qquad \text{for} \qquad m \geq 0 \tag{20}$$

we assume that the line goes through origin. In general if a real 2-D function has a definite direction then it's energy spectrum is concentrated to a line. Since the real functions Fourier coefficients should be Hermitian, their energy spectrum is even, forcing the line to pass through origin. This explains the model in (20). A real neighbourhood f can be evenly expanded in polar coordinates as before yielding:

$$f = \sum_{m,n \in Z} c_{mn} \Psi_{mn} = \sum_{m,n \in H} a_{mn} \phi_{mn}$$

real coefficients c_{mn}, a_{mn}. The neighbourhoods energy concentration in general degrades from a line through origin, Figure 2.9). Let us measure this by:

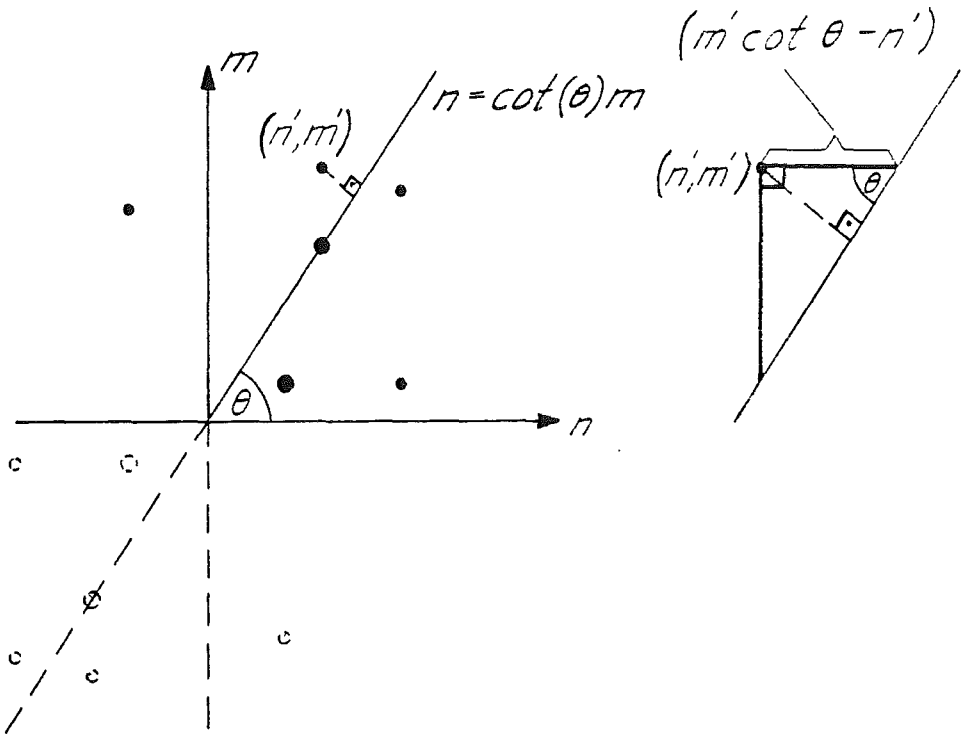

Figure 2.9) The least square fit of a line through origin to the spectrum of the input. The input is assumed to be real. Such an input should have a line concentration if it has a definite direction in polar spatial coordinates.

$$
\begin{aligned}
C_{\Omega\theta} &\triangleq \sum_{m,n\in H} (n-\cot(\theta)m)^2 \sin^2(\theta)\frac{a_{mn}^2}{A^2} = \sum_{m,n\in H} (n\sin(\theta)-m\cos(\theta))^2\frac{a_{mn}^2}{A^2} \\
&= \sin^2(\theta)\sum_{m,n\in H} n^2\frac{a_{mn}^2}{A^2} + \cos^2(\theta)\sum_{m,n\in H} m^2\frac{a_{mn}^2}{A^2} \\
&- \sin(2\theta)\sum_{m,n\in H} mn\frac{a_{mn}^2}{A^2}
\end{aligned} \tag{21}
$$

We want to find a θ which minimizes $C_{\Omega\theta}$. This is the least squares estimation of θ and it is straight forward to find it:

$$
\frac{dC_{\Omega\theta}}{d\theta} = (n_d^2 - m_d^2)\sin(2\theta) - 2p\cos(2\theta) \tag{22}
$$

where

$$
p = \sum_{m,n\in H} mn\frac{a_{mn}^2}{A^2}
$$

If $n_d^2 - m_d^2 \neq 0$ or $p \neq 0$ then

$$
\frac{dC_{\Omega\theta}}{d\theta} = \sqrt{(n_d^2 - m_d^2)^2 + 4p^2}\sin(2\theta - \theta_0) \tag{23}
$$

where θ_0 is such that

$$\sin(\theta_0) = \frac{2p}{\sqrt{(n_d^2 - m_d^2)^2 + 4p^2}} \tag{24}$$

$$\cos(\theta_0) = \frac{n_d^2 - m_d^2}{\sqrt{(n_d^2 - m_d^2)^2 + 4p^2}} \tag{25}$$

The fact that $\frac{dC_{\Omega\theta}}{d\theta} = 0$ when $\theta = \frac{\theta_0}{2}$ concludes the search of minimum together with

$$\begin{aligned} \frac{dC_{\Omega\theta}}{d\theta} &\leq 0 \quad \text{for} \quad \frac{\theta_0}{2} - \frac{\pi}{2} \leq \theta \leq \frac{\theta_0}{2} \\ \frac{dC_{\Omega\theta}}{d\theta} &\geq 0 \quad \text{for} \quad \frac{\theta_0}{2} \leq \theta \leq \frac{\theta_0}{2} + \frac{\pi}{2} \end{aligned}$$

Thus choose θ as $\frac{\theta_0}{2}$ and call it θ_d. This is delivered through

$$\theta_d = \frac{1}{2}\tan^{-1}(n_d^2 - m_d^2, 2p). \tag{26}$$

which is equivalent to the formula to (24) and (25): The error or the confidence measure is given by substituting (26) in (21) and observing the trigonometric half angle formulas in connection with (24) and (25):

$$C_{\Omega\theta} = \frac{1}{2}\left(n_d^2 + m_d^2 - \sqrt{(n_d^2 - m_d^2)^2 + 4p^2}\right). \tag{27}$$

The angle given by (26) gives the axis around which the moment of inertia is minimum and the moment of inertia is given by (27) if $\frac{a_{mn}{}^2}{A^2}$ is seen as a point mass, [7]. The omitted case when both $p = 0$ and $n_d^2 - m_d^2 = 0$ corresponds to the local neighbourhoods with no specific orientations. Because $\frac{dC_{\Omega\theta}}{d\theta}$ vanishes according to (22) indicating any θ would work as minimizing argument to (21). This case implies that

$$\begin{aligned} \sum_{m,n\in H} m^2 \frac{a_{mn}^2}{A^2} &= \sum_{m,n\in H} n^2 \frac{a_{mn}^2}{A^2} \\ \sum_{m,n\in H} mn \frac{a_{mn}^2}{A^2} &= 0 \end{aligned}$$

For example one class of functions having this property in their spectrums is the class of functions with equal masses at grid points with equal distances from origin in their spectrums. Neighbourhoods of ϕ_{00}, $\phi_{mn} + \phi_{-m-n}$ are examples of such functions. As an observation we

conclude that $m_d^2 = 0$ and $n_d^2 = 0$ implies that the neghborhood contains a constant function and we consequently have no orientation. Because if $m_d^2 = n_d^2 = 0$ then:

$$\|\frac{\partial f}{\partial r}\| = 0 \Longleftrightarrow \frac{\partial f}{\partial r} = 0$$
$$\|\frac{\partial f}{\partial \varphi}\| = 0 \Longleftrightarrow \frac{\partial f}{\partial \varphi} = 0$$

proving the statement. Thus to keep the consistency of the meaning of $C_{\Omega\theta}$ in the case when $n_d^2 - m_d^2 = p = 0$, we should define $C_{\Omega\theta} = \infty$ and leave θ undefined. n_d^2, m_d^2, p which are needed to calculate θ_d and $C_{\Omega\theta}$ according to (26) and (27), can easily be found in the spatial domain to be:

$$m_d^2 = \sum_{m,n\in H} \frac{a_{mn}^2}{A^2} = \frac{1}{A^2}\|\frac{\partial f}{\partial \varphi}\|^2$$
$$n_d^2 = \sum_{m,n\in H} n^2 \frac{a_{mn}^2}{A^2} = \frac{1}{A^2\omega^2}\|\frac{\partial f}{\partial r}\|^2$$
$$p = \sum_{m,n\in H} mn\frac{a_{mn}^2}{A^2} = \frac{1}{A^2\omega}(\frac{\partial f}{\partial r}, \frac{\partial f}{\partial \varphi})$$

Once we have a neighbourhood with the property of having a definite direction in polar coordinates, it is quite natural to try to render the behavior in this direction. We propose to depict the behavior of the spectrum by rendering it's point concentration, ν_d, in this direction:

$$\nu_d = \sqrt{m_d^2 + n_d^2} \tag{28}$$

we assumed that if there is a line concentration, then ν_d will give the position of it's point concentration. When we are interested only in the significance of the position of point concentration given by ν_d above without taking account to directionality existence the confidence measure,

$$C_{\Omega\omega} = C_{\Omega m} + C_{\Omega n} \tag{29}$$

should work for this purpose. Because $C_{\Omega\omega} = 0$ if and only if $C_{\Omega m} = C_{\Omega n} = 0$. But $C_{\Omega m} = 0$ if and only if the total energy is concentrated on a horizontal line and $C_{\Omega n} = 0$ if and only if the total energy is concentrated on a vertical line. The only chance for the neighbourhood to fulfill these requirements is being an input possessing total point concentration in it's spectrum, with location on the intersection of the lines $m = m_d$, $n = n_d$.

The set of the inputs with energy spectrum exhibiting concentration to a line and in addition exhibiting energy concentration to a point within this line is, a subset of the inputs with

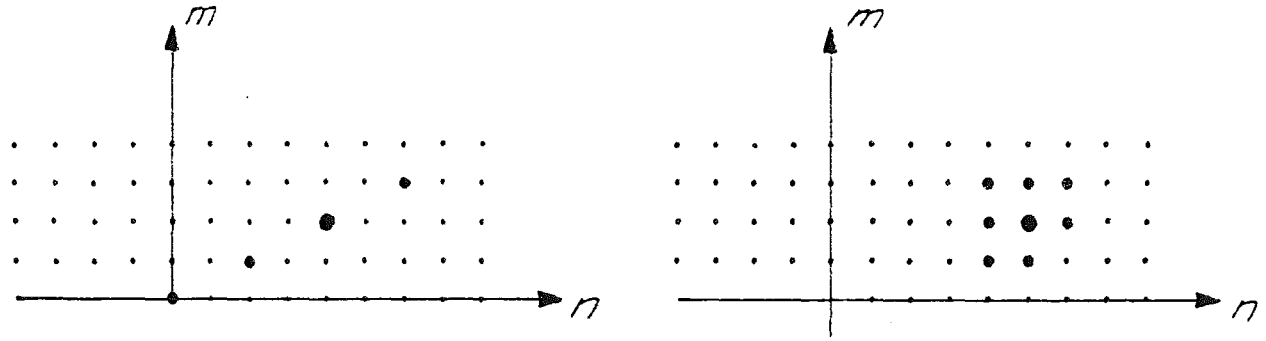

Figure 2.10) Two different types of point concentrations a) with directionality preference b) with non directional preference

energy concentration around this point, with no direction preference for the positions of the next largest components. Although the estimation of the position of the cluster, ν_d in (28) would work for both sets the confidence in the estimation, $C_{\Omega\omega}$, given in (29) should be different when we check the point concentration along a specific direction than when we check the point concentration. In the light of this discussion we propose the following expression for the confidence measure of direction specific point clustering, $C_{\Omega\nu}$:

$$C_{\Omega\nu} \triangleq C_{\Omega\theta} + C_{\Omega\omega} \tag{30}$$

$C_{\Omega\omega} \leq C_{\Omega\nu}$ since $C_{\Omega\theta}$, $C_{\Omega\omega} \geq 0$. This reflects the observation we made earlier: If the energy of an input is point concentrated on a line then it is also point concentrated, with no specific orientation preference. For the uncertainty increases by $C_{\Omega\theta}$, the uncertainty of line concentration, when we claim that ν_d is the position of point concentration in direction of θ.

When $C_{\Omega\theta} = 0$ then $C_{\Omega\nu} = C_{\Omega\omega}$ which means that the energy distribution on the line with angle θ sums up to total energy and the measure for energy variation within the line is the same as global variation, which is true. When $C_{\Omega\theta} = C_{\Omega\omega} = 0$ then $C_{\Omega\nu} = 0$ which reveals that we have a perfect concentration to a point and we are sure about the angle and magnitude of the position vector. This is in turn consistent with $C_{\Omega m} = C_{\Omega n} = 0$ including the case when we have only a constant input. Because we have $(m_d, n_d) = (0, 0)$ with total certainty.

With the propositions above, we have presented an additional measure for point concentration, this time it's position given in polar coordinates: θ_d and ν_d. The confidence parameter for θ_d is $C_{\Omega\theta}$. We have two choices for confidence parameters of ν_d influenced by whether we claim that the neighbourhood has direction specific point concentration or not. These are $C_{\Omega\nu}$ and $C_{\Omega\omega}$ respectively. In connection with these two choices, it is satisfactory to note that for a pure constant as input we get $C_{\Omega\nu} = \infty$ while $C_{\Omega\omega} = 0$.

CHAPTER 3
DESIGNING FILTERS FOR CIRCULAR SYMMETRY DETECTION

In this chapter we will propose methods for evaluating the neighbourhood dependent key numbers, necessary for the calculations of confidence and projection parameters mentioned in the previous chapter. Those key numbers were: (f,f), $(\frac{\partial f}{\partial r},\frac{\partial f}{\partial r})$, $(\frac{\partial f}{\partial \varphi},\frac{\partial f}{\partial \varphi})$, $(\frac{\partial f}{\partial r},\frac{\partial f}{\partial \varphi})$, $(\frac{\partial^2 f}{\partial r^2},\frac{\partial^2 f}{\partial r^2})$, $(\frac{\partial^2 f}{\partial \varphi^2},\frac{\partial^2 f}{\partial \varphi^2})$

The qualities these quantities share are

1) They are dependent upon the neighbourhood, Ω , in which the examined point lies.

2) They are operating upon the neighbourhoods belonging to $C^2(\Omega)$

3) They are applicable to every point in the picture.

For practical purposes, these properties introduce immense difficulties to the computational tractability of the evaluation of the key numbers if the following requirements are not fulfilled: 1) The key numbers should be possible to approximate with reasonable error by a discrete version of f. 2) Since these quantities are neighbourhood dependent and calculated in a similar manner for every point in the picture, they make considerable demands on computational throughput. Therefore the cost for mathematical operations involved should be low in the sense that the product *time demand* $\times$ *storage demand* for them is small.

We should remember, that f is the gray value function of the local neighbourhood, expressed in local coordinates. Moreover, it is also defined evenly for negative values of the radius through:

$$f(-r,\varphi) = f(r,-\varphi) \qquad (1).$$

It is easy to show that if a function h is even in polar coordinates as described in (1) then

$$(1,h) = \frac{1}{4\pi R}\int_{-\pi}^{\pi}\int_{-R}^{R} h(r,\varphi)\,dr\,d\varphi = \frac{1}{2\pi R}\int_{-\pi}^{\pi}\int_{0}^{R} h(r,\varphi)\,dr\,d\varphi$$

This is nothing but the scalar product defined in chapter 2) with

$$\Omega = [0, R] \otimes [0, 2\pi] \qquad (2).$$

Hence, when we calculate the scalar products in key quantities, we need to consider them as if Ω was given by (2). So we do not worry about the even periodization of local neighbourhood when we calculate$(f, f) = (1, f^2)$. We can pretend f to be the whole picture as long as the integration is carried out over the right part of the picture. We will come back to this translation problem soon. From now on we will assume that f is a 2-D continuous gray level function expressing the entire picture.

In the following it will be shown, that the referred quantities are possible to approximate by linear functionals operating on the sampled version of f, called $\hat{f}$ under certain circumstances. This leads us, naturally enough, to compute the key quantities through convolutions with fixed FIR-filters. These can preferably be computed on special machines capable of convolving sampled and digitized images with large kernels (GOP-300 for example) fast. Then one function, taking these quantities as arguments, can be constructed to deliver the confidence and projection parameters. Since this function is not neighbourhood dependent, one can allow a high degree of complexity relatively to neighbourhood dependent operations.

CALCULATION OF THE KEY QUANTITIES

Let us assume that f is sampled and that we omit the digitization errors caused by limited word length of the computers. Then we should somehow have access to information about the behavior of the image between the sampling points. To be reasonably general, and at the same time not run into undesirably heavy reconstruction problems, we assume that we are dealing with band limited images, which are sampled with sufficiently high degree of over sampling ratio. The latter is the ratio between sampling frequency and twice the maximum frequency of the image, e.g. Nyquist frequency. By this assumption we have, in fact, introduced one more error, because the patterns we are intending to detect and express are not band limited even though their Fourier transforms decay fast. We have to assume that they are band limited by some sort of filtering. Consequently, we will never, at least theoretically, be able to recognize any pattern we are trying to detect with zero uncertainty, but we can come very close to zero. We can decrease the amount of error caused by this source by sampling densely, hoping that this error is small compared to other sources we will mention below. Consequently we neglect this error type as well.

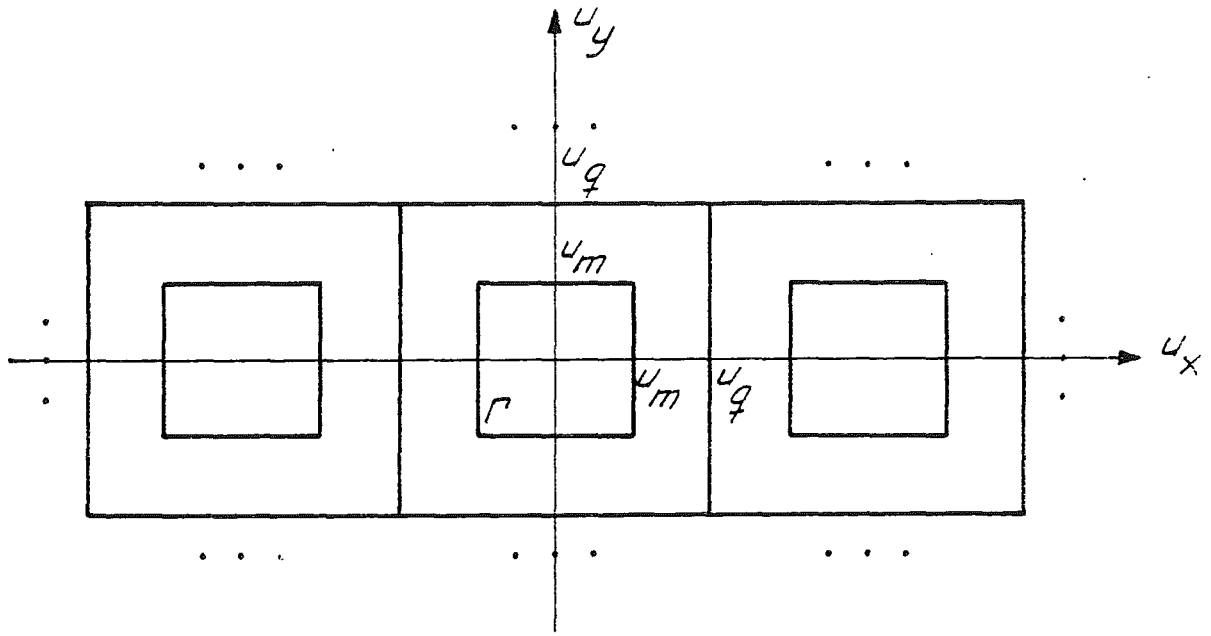

Figure 3.1): F(f) is assumed to vanish outside of the square, Γ. This allows us to sample f with the over sampling rate $\frac{f_q}{f_m}$, causing the dashed repetition pattern.

Since f is band limited, one can reconstruct f, from it's sampled version $\hat{f}$

$$\hat{f}(\bar{r}) = \sum_{i,j \in B} f(\bar{r}_{ij}) \delta(\bar{r} - \bar{r}_{ij}) \tag{3}$$

B is the set of integers labelling the sampling points, $\bar{r}_{ij}$, of the continuous picture f. B is assumed to be a square grid. $\delta(\bar{r})$ is the Dirac distribution. Since a rectangular sampling corresponds to repetition of the Fourier transform in a rectangular manner, the reconstruction can be carried out by convolving $\hat{f}$ with the inverse Fourier transform of the function

$$\Lambda(\bar{u}) = \begin{cases} 1, & \text{if } \bar{u} \in \Gamma; \\ 0, & \text{otherwise.} \end{cases}$$

yielding

$$f(\bar{r}) = \hat{f} * \left[\mathcal{F}^{-1}(\Lambda)\right] \tag{4}$$

where $\bar{u}$ is the coordinate vector of the Fourier transform domain, Γ is the closed domain in which $\mathcal{F}(f)$ does not vanish, within the repetition zone, figure 3.1).

For the sake of simplicity, we will assume a square Γ, centered in the repetition square. u_q is the maximum allowable frequency in vertical and horizontal direction, not causing sampling

distortion. u_m is the actual limit for maximum frequencies of the picture f in horizontal and vertical direction. But by assuming Γ being completely in the repetition zone, we can write:

$$\begin{aligned}\lambda(\bar{r}) = \mathcal{F}^{-1}(\bar{r}) &= \int_{-u_q}^{u_q}\int_{-u_q}^{u_q} e^{i2\pi(u_x x+u_y y)}du_x u_y \\ &= \frac{\sin(2\pi u_q x)}{\pi x}\frac{\sin(2\pi u_q y)}{\pi y}\end{aligned} \tag{5}$$

As the maximum allowable frequency is f_q we get the sampling period as (Nyquist criteria)

$$T = \frac{1}{2u_q}$$

For simplicity we put $T = 1$ and this causes u_q to be $\frac{1}{2}$. The reconstruction of f from it's samples yields through (3), (4), (5):

$$\begin{aligned}f(\bar{r}) &= \sum_{i,j\in B} f(\bar{r}_{ij})(\delta(\bar{r}-\bar{r}_{ij}) * \lambda(\bar{r})) = \sum_{i,j\in B} f(\bar{r}_{ij})(\delta(\bar{r}) * \lambda(\bar{r}-\bar{r}_{ij})) \\ &= \sum_{i,j\in B} f(\bar{r}_{ij})\lambda(\bar{r}-\bar{r}_{ij})\end{aligned} \tag{6}$$

In the previous chapter we have modelled operations delivering scalar values at the examined point. The scalar product and neighbourhood Ω, were connected to this point. In the following we propose methods for computing key quantities at a number of points. Consequently we need to attach a variable $\bar{r}$ to the examined point, which is assumed to have the coordinate vector $\bar{r}$ and dependent quantities:

$$\Omega_{\bar{r}} \triangleq \{\bar{r}' : \quad |\bar{r}' - \bar{r}| \leq R\}$$

$$(f,g)_{\bar{r}} = \int_{\Omega\bar{r}} \frac{1}{|\bar{r}'-\bar{r}|} f^*(\bar{r}')g(\bar{r}')d\Omega_{\bar{r}}$$

1) Evaluation of (f,f)

(f,f), the energy of the local neighbourhood in terms of the scalar product defined in the previous chapter, can be found by using the reconstruction formula in (6) for f^2, provided that $\frac{u_q}{u_m} > 2$. Because $\mathcal{F}(f^2) = \mathcal{F}(f) * \mathcal{F}(f)$, which implies that the non vanishing area of $\mathcal{F}(f^2)$ is quadrupled. Thus, to guarantee non distorted image retrieval, we should impose the condition $\frac{u_q}{u_m} > 2$, resulting in:

$$
\begin{aligned}
(f,f)_{\bar{r}} = (1,f^2)_{\bar{r}} &= \Big(1, \sum_{i,j\in B} f^2(\bar{r}_{ij})\lambda(\bar{r}' - \bar{r}_{ij})\Big)_{\bar{r}} \\
&= \sum_{i,j\in B} f^2(\bar{r}_{ij})(1, \lambda(\bar{r}' - \bar{r}_{ij}))_{\bar{r}}
\end{aligned} \tag{7}
$$

We have now transformed our scalar product to an ordinary scalar product between two vectors in a finite dimensional Euclidean space. As the version of f is sampled, the picture is assumed to have finite extent. The vectors, call them $\overline{f^2}$ and $\bar{\alpha}(\bar{r})$ have the components:

$$
(\overline{f^2})_{ij} \triangleq f^2(\bar{r}_{ij})
$$

$$
(\bar{\alpha}(\bar{r}))_{ij} \triangleq \big(1, \lambda(\bar{r}' - \bar{r}_{ij})\big)_{\bar{r}}
$$

Having these definitions in mind we establish that $(f,f)_{\bar{r}}$ can be evaluated through an ordinary scalar product in the Euclidean space made by the sampled images:

$$
(f,f)_{\bar{r}} = (\overline{f^2})^t \bar{\alpha}(\bar{r}) \tag{8}
$$

(8) suggests to carry out the computation through a weighted sum of a new picture, $\overline{f^2}$ but the weighting coefficients are dependent of the examined point. The fact that they are as many as the picture samples does not make the computation of all $\big(f,f\big)_{\bar{r}_{ij}}$ for $i,j \in B$, easier.

We are going to approximate (8) on the basis of the following observation: The weighting coefficients, $(\bar{\alpha}(\bar{r}))_{ij}$, in general will decrease when $|\bar{r} - \bar{r}_{ij}|$ increases, due to fix potential $\frac{1}{r}$ and decaying λ.

Thus (7) can be approximated by taking only those coefficients with $\bar{r}$ closest to $\bar{r}$

Let this approximation be done by the vector $\hat{\alpha}(\bar{r})$:

$\hat{\alpha}(\bar{r}) + \bar{\epsilon}_{\alpha}(\bar{r})$

where

$$
(\hat{\alpha}(\bar{r}))_{ij} = \begin{cases} (\bar{\alpha}(\bar{r}))_{ij}, & \text{if } |\bar{r} - \bar{r}_{ij}| \le R'; \\ 0, & \text{otherwise.} \end{cases} \tag{9}
$$

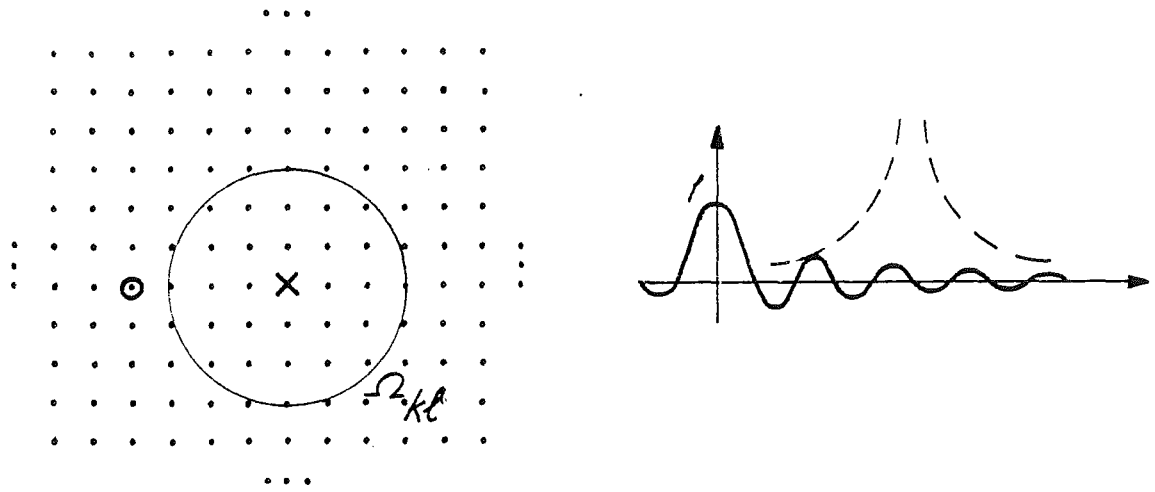

Figure 3.2) To the left we have the grid of the discretization points. The cross marks the examined point $\bar{r}$, the circle marks the location where $\lambda(\bar{r}-\bar{r}_{ij})$ is centered, $\bar{r}_{ij}$. Then $(\bar{\alpha}(\bar{r}))_{ij}$ is evaluated by integrating $\lambda(\bar{r}-\bar{r}_{ij})$ at $\Omega_{\bar{r}}$ with a factor of $\frac{1}{r}$. To the right we have the profile of the damped sine, $\lambda(\bar{r}-\bar{r}_{ij})$, together with the integrating factor $\frac{1}{|\bar{r}-\bar{r}_{ij}|}$

Thus $\hat{\alpha}(\bar{r})$ is nonzero inside a circular mask, call it Ω', centered at $\bar{r}$. Since the components of $\bar{\alpha}(\bar{r})$ are integrals over translated functions we can write:

$$\begin{aligned}(\bar{\alpha}(\bar{r}))_{ij} &= \frac{1}{2\pi R}\int_{\Omega_{\bar{r}}}\frac{1}{|\bar{r}'-\bar{r}|}\lambda(\bar{r}'-\bar{r}_{ij})d\Omega_{\bar{r}} \\ &= \frac{1}{2\pi R}\int_0^{2\pi}\int_0^R \frac{\sin(\pi(r'\cos\varphi'-x_i-x))}{\pi(r'\cos\varphi'-x_i-x)}\frac{\sin(\pi(r'\sin\varphi'-y_i-y))}{\pi(r'\sin\varphi'-y_i-y)}dr'd\varphi' \qquad (10)\\ &= \big(1,\lambda(\bar{r}'-\bar{r}_{ij}-\bar{r})\big)_{\bar{0}}\end{aligned}$$

If $\bar{r}$ is chosen as one of $\{\bar{r}_{ij}\}_{ij\in B}$ we can write:

$$\big(\bar{\alpha}(\bar{r}_{kl})_{ij} = \big(\bar{\alpha}(\bar{0})\big)_{(k+i)(l+j)}$$

Since $\bar{r}_{ij}=(i,j)$. This leads to

$$\big(f,f\big)_{\bar{r}} = \sum_{i,j\in B}\big(\hat{\alpha}(\bar{0})\big)_{(k+i),(l+j)}\big(\overline{f^2}\big)_{ij} + \sum_{i,j\in B}\big(\bar{\epsilon}(\bar{0})\big)_{(k+i)(l+j)}\big(\overline{f^2}\big)_{ij} \qquad (11)$$

R	R'	σ_α
6.0	9	0.005
7.0	10	0.003
8.0	11	0.004

R	R'	σ_β
6.0	9	0.004
7.0	10	0.004
8.0	11	0.003

Table 3.1): The relative errors made by truncating $\bar{\alpha}$ and $\bar{\beta}$.

which is a discrete convolution by fixed coefficient vectors. The error we do when we put:

$$(f,f)_{\bar{r}_{kl}} \approx \sum_{i,j\in B} \left(\hat{\alpha}(\bar{0})\right)_{(k+i)(l+j)} \left(\overline{f^2}\right)_{ij} \tag{12}$$

is naturally dependent on $\hat{f^2}$. But the error in approximation of $\bar{\alpha}(\bar{0})$ is $\bar{\epsilon}(\bar{0})$ and we choose $\|.\|_\infty$ to express the norm of both vectors, because it is easy to compute:

$$\|\bar{\alpha}(\bar{0})\|_\infty = \left|\bar{\alpha}(\bar{0})_{i'j'}\right|$$

where $\bar{\alpha}(\bar{0})_{i'j'}$ is the component of $\bar{\alpha}(\bar{0})$ with largest magnitude. Define a relative error σ_α as

$$\sigma_\alpha = \frac{\|\bar{\epsilon}_\alpha(\bar{0})\|_\infty}{\|\bar{\alpha}(\bar{0})\|_\infty}$$

The maximum norm is found by inspection of $\left(\bar{\alpha}(\bar{0})\right)_{ij}$ for which the required integrations are computed numerically only at some critical i,j's thanks to the symmetry of $\left(\bar{\alpha}(\bar{0})\right)_{ij}$. We have also used the knowledge of decaying behavior of $\left(\bar{\alpha}(\bar{0})\right)_{ij}$ to avoid to compute these at very large i,j's, table 3.1). The numerical computation for the double integrals are carried out by assuming the inner integral as a new integrand to the outer one. The obtained one-dimensional integrations are carried out by using subroutines from the SLATEC subroutine package using adaptive quadrature schemes on a VAX computer.

2) $\left(\frac{\partial f}{\partial r'}, \frac{\partial f}{\partial r'}\right)_{\bar{r}}$

Since we have access to only rectangular sampling we should transform the partial derivatives with respect to r, to be derivatives with respect to local cartesian coordinates. The

inconvenience of partial derivatives with respect to local polar coordinates is seen by considering a point $\bar{r}'$ belonging to two overlapping neighbourhoods $\Omega_{\bar{r}_0}$, $\Omega_{\bar{r}_1}$. Then the radial partial derivative $\frac{\partial f}{\partial r}$ is changed from $\Omega_{\bar{r}_0}$ to $\Omega_{\bar{r}_1}$, whereas $\frac{\partial f}{\partial x}$ and $\frac{\partial f}{\partial y}$ remain unchanged, leading to shift invariance of the partial derivatives under a shift of the neighbourhood, a property which is essential for convolution based realizations. Thus we consider the following well-known transformations in local coordinates:

$$x' = r' \cos(\varphi')$$
$$y' = r' \sin(\varphi')$$

Here r' and φ' are polar coordinates of any point in the picture relative to the examined point, while x' and y' are the corresponding cartesian ones.

$$\frac{\partial f}{\partial r'} = \frac{\partial f}{\partial r'} \cos(\varphi') + \frac{\partial f}{\partial y'} \sin(\varphi') \tag{13}$$

yielding:

$$\left(\frac{\partial f}{\partial r'}, \frac{\partial f}{\partial r'}\right)_{\bar{r}} = \left(\cos^2(\varphi'), \left(\frac{\partial f}{\partial x'}\right)^2\right)_{\bar{r}} + \left(\sin^2(\varphi'), \left(\frac{\partial f}{\partial y'}\right)^2\right)_{\bar{r}} + \left(\sin^2(\varphi'), \frac{\partial f}{\partial x'}\frac{\partial f}{\partial y'}\right)_{\bar{r}} \tag{14}.$$

Remembering that the product of two band limited functions has an increased band width (due to the convolution in the frequency domain), and partial derivations with respect to horizontal and vertical components do not enlarge the nonzero areas, we should be able to write:

$$\left(\cos^2(\varphi'), \left(\frac{\partial f}{\partial x'}\right)^2\right)_{\bar{r}} = \sum_{i,j \in B} \left(\frac{\partial f}{\partial x}\right)^2\Big|_{\bar{r}_{ij}} \left(\cos^2(\varphi'), \lambda(\bar{r}' - \bar{r}_{ij})\right)_{\bar{r}} \tag{15}$$

with the special requirement for our square non vanishing area, Γ, in the frequency domain:

$$\frac{u_q}{u_m} > 2 \tag{16}$$

as before. Similarly under the condition (16) the other two components involved in (14), necessary for evaluation of the energy of $\frac{\partial f}{\partial r}$ can be written as:

$$\left(\sin^2(\varphi'), (\frac{\partial f}{\partial y'})^2\right)_{\bar{r}} = \sum_{i,j \in B} (\frac{\partial f}{\partial y})^2\big|_{\bar{r}_{ij}} \left(\sin(2\varphi'), \lambda(\bar{r}' - \bar{r}_{ij})\right)_{\bar{r}} \tag{17}$$

$$\left(\sin(2\varphi'), \frac{\partial f}{\partial x'}\frac{\partial f}{\partial y'}\right)_{\bar{r}} = \sum_{i,j \in B} (\frac{\partial f}{\partial x}\frac{\partial f}{\partial y})\big|_{\bar{r}_{ij}} \left(\sin(2\varphi'), \lambda(\bar{r}' - \bar{r}_{ij})\right)_{\bar{r}} \tag{18}$$

where $f\big|_{\bar{r}_{ij}}$ means the value of f at the point $\bar{r}_{ij}$. (15), (17) and (18) are then reduced to three ordinary scalar products between two vectors in a finite dimensional euclidean space, since $(\frac{\partial f}{\partial x})^2$, $(\frac{\partial f}{\partial y})^2$, $\frac{\partial f}{\partial x}\frac{\partial f}{\partial y}$ are band limited and the samples of f have limited extent. The three vectors originating from the pictures of cartesian partial derivatives with the component indexes ij:

$$\left(\overline{f_x^2}\right)_{ij} \triangleq (\frac{\partial f}{\partial x})^2\big|_{\bar{r}_{ij}}$$

$$\left(\overline{f_y^2}\right)_{ij} \triangleq (\frac{\partial f}{\partial y})^2\big|_{\bar{r}_{ij}}$$

$$\left(\overline{f_x f_y}\right)_{ij} \triangleq (\frac{\partial f}{\partial x}\frac{\partial f}{\partial y})\big|_{\bar{r}_{ij}}$$

are all independent of the examined point. However, the other three vectors $\bar{\beta}(\bar{r})$, $\bar{\gamma}(\bar{r})$, $\bar{\varsigma}(\bar{r})$ with component indexes ij:

$$\left(\bar{\beta}(\bar{r})\right)_{ij} \triangleq \left(\cos^2(\varphi'), \lambda(\bar{r}' - \bar{r}_{ij})\right)_{\bar{r}} \tag{19}$$

$$\left(\bar{\gamma}(\bar{r})\right)_{ij} \triangleq \left(\sin^2(\varphi'), \lambda(\bar{r}' - \bar{r}_{ij})\right)_{\bar{r}} \tag{20}$$

$$\left(\bar{\varsigma}(\bar{r})\right)_{ij} \triangleq \left(\sin(2\varphi'), \lambda(\bar{r}' - \bar{r}_{ij})\right)_{\bar{r}} \tag{21}$$

are not. They are dependent on the difference $\bar{r}-\bar{r}_{ij}$. In analogy with the $(f,f)_{\bar{r}}$ computation we observe that (19), (20) and (21) decay when $|\bar{r}_{ij}-\bar{r}|$ increases. We will utilize this property to approximate, (14), :

$$(\frac{\partial f}{\partial r'},\frac{\partial f}{\partial r'})_{\bar{r}} = \bar{\beta}(\bar{r})^t\overline{f_x^2} + \bar{\gamma}(\bar{r})^t\overline{f_y^2} + \bar{\varsigma}(\bar{r})^t\overline{f_x f_y} \tag{22}$$

through the equation:

$$(\frac{\partial f}{\partial r'},\frac{\partial f}{\partial r'})_{\bar{r}} = \big(\hat{\beta}(\bar{r})+\bar{\epsilon}_\beta(\bar{r})\big)^t\overline{f_x^2} + \big(\hat{\gamma}(\bar{r})+\bar{\epsilon}_\gamma(\bar{r})\big)^t\overline{f_y^2} + \big(\hat{\varsigma}(\bar{r})+\bar{\epsilon}_\varsigma(\bar{r})\big)^t\overline{f_x f_y} \tag{23}$$

Here we have split up $\bar{\beta}(\bar{r})$ to two vectors, where $\hat{\beta}(\bar{r})$ components are

$$\big(\hat{\beta}(\bar{r})\big)_{ij} = \begin{cases} \big(\bar{\beta}(\bar{r})\big)_{ij}, & \text{if } |\bar{r}-\bar{r}_{ij}| \le R'; \\ 0, & \text{otherwise.} \end{cases} \tag{24}$$

in such a way that

$$\bar{\beta}(\bar{r}) = \hat{\beta}(\bar{r}) + \bar{\epsilon}_\beta(\bar{r}).$$

The same is carried out for $\bar{\gamma}$ and $\bar{\varsigma}$. This leads us to

$$\begin{aligned} \big(\hat{\beta}(\bar{r}_{kl})\big)_{ij} &= \big(\hat{\beta}(\bar{0})\big)_{(i-k)(j-l)} \\ \big(\hat{\gamma}(\bar{r}_{kl})\big)_{ij} &= \big(\hat{\gamma}(\bar{0})\big)_{(i-k)(j-l)} \\ \big(\hat{\varsigma}(\bar{r}_{kl})\big)_{ij} &= \big(\hat{\varsigma}(\bar{0})\big)_{(i-k)(j-l)} \end{aligned} \tag{25}$$

and

$$\begin{aligned} \sigma_\beta &\triangleq \frac{\|\bar{\epsilon}_\beta(\bar{0})\|_\infty}{\|\bar{\beta}(\bar{0})\|_\infty} \\ \sigma_\gamma &\triangleq \frac{\|\bar{\epsilon}_\gamma(\bar{0})\|_\infty}{\|\bar{\gamma}(\bar{0})\|_\infty} \\ \sigma_\varsigma &\triangleq \frac{\|\bar{\epsilon}_\varsigma(\bar{0})\|_\infty}{\|\bar{\varsigma}(\bar{0})\|_\infty} \end{aligned} \tag{26}$$

as before. If we define $\sigma_{\beta\gamma\varsigma}$ as

$$\sigma_{\beta\gamma\varsigma} \stackrel{\triangle}{=} \sigma_\beta + \sigma_\gamma + \sigma_\varsigma$$

we can use this as a norm for the error made in the operations of (22). This will express how well we have managed to do our total approximation through separate approximations when we adopt:

$$\begin{aligned}\left(\frac{\partial f}{\partial \bar{r}'}, \frac{\partial f}{\partial \bar{r}'}\right)_{\bar{r}_{kl}} \approx \sum_{i,j\in B} &\left(\hat{\beta}(\bar{r}_{kl})\right)_{(k+i)(l+j)} \overline{(f_x^2)}_{ij} + \left(\hat{\gamma}(\bar{r}_{kl})\right)_{(k+i)(l+j)} \overline{(f_y^2)}_{ij} \\ &+ \left(\hat{\varsigma}(\bar{r}_{kl})\right)_{(k+i)(l+j)} \overline{(f_x f_y)}_{ij}\end{aligned} \tag{27}$$

3) $\left(\frac{\partial f}{\partial \varphi'}, \frac{\partial f}{\partial \varphi'}\right)_{\bar{r}}$

As in the previous case, through the partial derivation:

$$\frac{\partial f}{\partial \varphi'} = -\frac{\partial f}{\partial x'} r' \sin(\varphi') + \frac{\partial f}{\partial y'} r' \cos(\varphi') \tag{28}$$

we get

$$\left(\frac{\partial f}{\partial \varphi'}, \frac{\partial f}{\partial \varphi'}\right)_{\bar{r}} = \left(r'^2 \sin^2(\varphi'), \left(\frac{\partial f}{\partial x'}\right)^2\right)_{\bar{r}} + \left(r'^2 \cos^2(\varphi'), \left(\frac{\partial f}{\partial y'}\right)^2\right)_{\bar{r}} - \left(r'^2 \sin(2\varphi'), \frac{\partial f}{\partial x'} \frac{\partial f}{\partial y'}\right)_{\bar{r}} \tag{29}$$

We use the band limitation assumption for the involved pictures and find:

$$\begin{aligned}\left(r'^2 \sin^2(\varphi'), \left(\frac{\partial f}{\partial x'}\right)^2\right)_{\bar{r}} &= \sum_{i,j\in B} \left(\frac{\partial f}{\partial x}\right)^2\Big|_{\bar{r}_{ij}} \left(r'^2 \sin^2(\varphi'), \lambda(\bar{r}' - \bar{r}_{ij})\right)_{\bar{r}} \\ \left(r'^2 \cos^2(\varphi'), \left(\frac{\partial f}{\partial y'}\right)^2\right)_{\bar{r}} &= \sum_{i,j\in B} \left(\frac{\partial f}{\partial y}\right)^2\Big|_{\bar{r}_{ij}} \left(r'^2 \cos^2(\varphi'), \lambda(\bar{r}' - \bar{r}_{ij})\right)_{\bar{r}} \\ \left(r'^2 \sin(2\varphi'), \frac{\partial f}{\partial x'} \frac{\partial f}{\partial y'}\right)_{\bar{r}} &= \sum_{i,j\in B} \left(\frac{\partial f}{\partial x} \frac{\partial f}{\partial y}\right)\Big|_{\bar{r}_{ij}} \left(r'^2 \sin(2\varphi'), \lambda(\bar{r}' - \bar{r}_{ij})\right)_{\bar{r}}\end{aligned} \tag{30}$$

We define the vectors $\bar{\eta}(\bar{r})$, $\bar{\kappa}(\bar{r})$, $\bar{\mu}(\bar{r})$ through their components as

R	R'	σ_ς
6.0	7	0.001
7.0	10	0.004
8.0	8	0.004

R	R'	σ_η
6.0	11	0.015
7.0	11	0.021
8.0	11	0.028

Table 3.2): The relative errors made by truncating $\bar{\varsigma}$ and $\bar{\eta}$.

$$\begin{aligned}
\big(\bar{\eta}(\bar{r})\big)_{ij} &\triangleq \big(r'^2\sin^2(\varphi'), \lambda(\bar{r}' - \bar{r}_{ij})\big)_{\bar{r}} \\
\big(\bar{\kappa}(\bar{r})\big)_{ij} &\triangleq \big(r'^2\cos^2(\varphi'), \lambda(\bar{r}' - \bar{r}_{ij})\big)_{\bar{r}} \\
\big(\bar{\mu}(\bar{r})\big)_{ij} &\triangleq \big(r'^2\sin(2\varphi'), \lambda(\bar{r}' - \bar{r}_{ij})\big)_{\bar{r}}
\end{aligned} \tag{31}$$

$$\big(\frac{\partial f}{\partial \varphi'}, \frac{\partial f}{\partial \varphi'}\big)_{\bar{r}} = \bar{\eta}(\bar{r})^t\overline{f_x^2} + \bar{\kappa}(\bar{r})^t\overline{f_y^2} - \bar{\mu}(\bar{r})^t\overline{f_x f_y} \tag{32}$$

We approximate $\bar{\eta}(\bar{r})$, $\bar{\kappa}(\bar{r})$, $\bar{\mu}(\bar{r})$ by $\hat{\eta}(\bar{r})$, $\hat{\kappa}(\bar{r})$, $\hat{\mu}(\bar{r})$ with the errors $\bar{\epsilon}_\eta(\bar{r})$, $\bar{\epsilon}_\kappa(\bar{r})$, $\bar{\epsilon}_\mu(\bar{r})$. The approximation technique is the same as before, that is $\bar{\eta}(\bar{r})$, $\bar{\kappa}(\bar{r})$, $\bar{\mu}(\bar{r})$ are put to zero when $|\bar{r}_{ij} - \bar{r}| > R'$ to obtain $\hat{\eta}(\bar{r})$, $\hat{\kappa}(\bar{r})$, $\hat{\mu}(\bar{r})$ resulting in convolutions:

$$\begin{aligned}
\big(\frac{\partial f}{\partial \varphi'}, \frac{\partial f}{\partial \varphi'}\big)_{\bar{r}_{kl}} \approx \sum_{i,j\in B} &\big(\hat{\eta}(\bar{r}_{kl})\big)_{(k+i)(l+j)}\big(\overline{f_x^2}\big)_{ij} + \big(\hat{\kappa}(\bar{r}_{kl})\big)_{(k+i)(l+j)}\big(\overline{f_y^2}\big)_{ij} \\
&+ \big(\hat{\mu}(\bar{r}_{kl})\big)_{(k+i)(l+j)}\big(\overline{f_x f_y}\big)_{ij}
\end{aligned} \tag{33}$$

with the error definitions

$$\begin{aligned}
\sigma_\eta &\triangleq \frac{\|\bar{\epsilon}_\eta(\bar{0})\|_\infty}{\|\bar{\eta}(\bar{0})\|_\infty} \\
\sigma_\kappa &\triangleq \frac{\|\bar{\epsilon}_\kappa(\bar{0})\|_\infty}{\|\bar{\kappa}(\bar{0})\|_\infty} \\
\sigma_\mu &\triangleq \frac{\|\bar{\epsilon}_\mu(\bar{0})\|_\infty}{\|\bar{\mu}(\bar{0})\|_\infty} \\
\sigma_{\eta\kappa\mu} &\triangleq \sigma_\eta + \sigma_\kappa + \sigma_\mu
\end{aligned} \tag{34}$$

The approximation errors are only given for $\bar{\varsigma}$ and $\bar{\eta}$ in the table 3.2) and table 3.3), because of symmetry.

We have in the previous chapter referred to a variable *sign* telling us whether the proposed point concentration measure n_d^2 is in the left half plane or the right half plane of H. We will do that by checking the sign of

$$p = \frac{1}{A^2\omega}\left(\frac{\partial f}{\partial r}, \frac{\partial f}{\partial \varphi}\right)_{\bar{r}_{kl}} = \sum_{m,n\in H} mn\frac{a_{mn}^2}{A^2}$$

telling us which half plane is more dominant. We will evaluate this quantity, which was necessary also for the line concentration case.

4) $\left(\frac{\partial f}{\partial r'}, \frac{\partial f}{\partial \varphi'}\right)_{\bar{r}}$

The approximation is based on the equation obtained by (13) and 28):

$$\frac{\partial f}{\partial r'}\frac{\partial f}{\partial \varphi'} = -\frac{1}{2}\left(\frac{\partial f}{\partial x'}\right)^2 r'\sin(2\varphi') + \frac{1}{2}\left(\frac{\partial f}{\partial y'}\right)^2 r'\sin(2\varphi') + \frac{\partial f}{\partial x'}\frac{\partial f}{\partial y'}r'\cos(2\varphi') \tag{35}$$

yielding

$$\left(\frac{\partial f}{\partial r'}, \frac{\partial f}{\partial \varphi'}\right)_{\bar{r}} = -\frac{1}{2}\left(r'\sin(2\varphi'), \left(\frac{\partial f}{\partial x'}\right)^2\right)_{\bar{r}} + \frac{1}{2}\left(r'\sin(2\varphi'), \left(\frac{\partial f}{\partial y'}\right)^2\right)_{\bar{r}} + \left(r'\cos(2\varphi'), \frac{\partial f}{\partial x'}\frac{\partial f}{\partial y'}\right)_{\bar{r}} \tag{36}$$

after discussions appearing earlier in 1), 2), 3) one obtains:

$$\left(\frac{\partial f}{\partial r'}, \frac{\partial f}{\partial \varphi'}\right)_{\bar{r}} = -\frac{1}{2}\bar{\nu}(\bar{r})^t\overline{f_x^2} + \frac{1}{2}\bar{\nu}(\bar{r})^t\overline{f_y^2} + \bar{\tau}(\bar{r})^t\overline{f_x f_y} \tag{37}$$

with

$$\begin{aligned}\left(\bar{\nu}(\bar{r})\right)_{ij} &\triangleq \left(r'\sin(2\varphi'), \lambda(\bar{r}' - \bar{r}_{ij})\right)_{\bar{r}} \\ \left(\bar{\tau}(\bar{r})\right)_{ij} &\triangleq \left(r'\cos(2\varphi'), \lambda(\bar{r}' - \bar{r}_{ij})\right)_{\bar{r}}\end{aligned} \tag{38}$$

Then the approximation is immediate with the error performance given in table 3.3) as

R	R'	σ_μ
6.0	11	0.004
7.0	13	0.004
8.0	8	0.004

R	R'	σ_τ
6.0	11	0.012
7.0	11	0.018
8.0	11	0.025

Table 3.3): The relative errors made by truncating $\bar{\mu}$ and $\bar{\tau}$.

$$\left(\frac{\partial f}{\partial r'}, \frac{\partial f}{\partial \varphi'}\right)_{\bar{r}_{kl}} \approx \sum_{i,j \in B} \frac{1}{2}\left(\hat{\nu}(\bar{0})\right)_{(k+i)(l+j)}\left(\left(\overline{f_y^2}\right)_{ij} - \left(\overline{f_x^2}\right)_{ij}\right) + \left(\hat{\tau}(\bar{0})\right)_{(k+i)(l+j)}\left(\overline{f_x f_y}\right)_{ij} \quad (39)$$

where the $\hat{\nu}(\bar{0})$, $\hat{\tau}(\bar{0})$ are analogous to similar vectors given earlier.

5) $\left(\frac{\partial^2 f}{\partial r'^2}, \frac{\partial^2 f}{\partial r'^2}\right)_{\bar{r}}$

We will express the partial derivatives with respect to polar coordinates in partial derivatives with respect to cartesian coordinates and use the chain rule in 13):

$$\begin{aligned} \frac{\partial^2 f}{\partial r'^2} &= \cos\varphi' \frac{\partial}{\partial x'}\left(\cos\varphi' \frac{\partial f}{\partial x'} + \sin\varphi' \frac{\partial f}{\partial y'}\right) + \\ &\quad \sin\varphi' \frac{\partial}{\partial y'}\left(\cos\varphi' \frac{\partial f}{\partial x'} + \sin\varphi' \frac{\partial f}{\partial y'}\right) \\ &= \cos^2\varphi' \frac{\partial^2 f}{\partial x'^2} + \sin^2\varphi' \frac{\partial^2 f}{\partial y'^2} \sin 2\varphi' \frac{\partial^2 f}{\partial x' \partial y'} \end{aligned} \quad (40)$$

Thus

$$\begin{aligned} \left(\frac{\partial^2 f}{\partial r'^2}, \frac{\partial^2 f}{\partial r'^2}\right)_{\bar{r}} &= \left(1, \left(\frac{\partial^2 f}{\partial r'^2}\right)^2\right)_{\bar{r}} \\ &= \left(\cos^4\varphi', \left(\frac{\partial^2 f}{\partial x'^2}\right)^2\right)_{\bar{r}} + \left(\sin^4\varphi', \left(\frac{\partial^2 f}{\partial y'^2}\right)^2\right)_{\bar{r}} + \left(\sin^2 2\varphi', \left(\frac{\partial^2 f}{\partial x' \partial y'}\right)^2\right)_{\bar{r}} \\ &= +\frac{1}{2}\left(\sin^2 2\varphi', \frac{\partial^2 f}{\partial x'^2} \cdot \frac{\partial^2 f}{\partial y'^2}\right)_{\bar{r}} + 2\left(\cos^2\varphi' \sin 2\varphi', \frac{\partial^2 f}{\partial x'^2} \frac{\partial^2 f}{\partial x' \partial y'}\right)_{\bar{r}} \\ &\quad + 2\left(\sin^2\varphi' \sin 2\varphi', \frac{\partial^2 f}{\partial y'^2} \frac{\partial^2 f}{\partial x' \partial y'}\right)_{\bar{r}} \end{aligned} \quad (41)$$

The straightforward application of the band limited functions theory, as before, produces:

R	R'	σ_{ρ_1}
6.0	9	0.005
7.0	10	0.005
8.0	11	0.004

R	R'	σ_{v_2}
6.0	11	0.020
7.0	11	0.026
8.0	11	0.035

Table 3.4): The relative errors made by truncating $\bar{\rho}_1$ and $\bar{v}_2$.

$$\begin{aligned}\left(\frac{\partial^2 f}{\partial r'^2}, \frac{\partial^2 f}{\partial r'^2}\right)_{\bar{r}} \approx & \sum_{i,j\in B} \left(\hat{\rho}_1(\bar{0})\right)_{(k+i)(l+j)} \left(\overline{f_{xx}^2}\right)_{ij} + \sum_{i,j\in B} \left(\hat{\rho}_2(\bar{0})\right)_{(k+i)(l+j)} \left(\overline{f_{yy}^2}\right)_{ij} + \\ & \sum_{i,j\in B} \left(\hat{\rho}_3(\bar{0})\right)_{(k+i)(l+j)} \left(\overline{f_{xy}^2}\right)_{ij} + \frac{1}{2} \sum_{i,j\in B} \left(\hat{\rho}_3(\bar{0})\right)_{(k+i)(l+j)} \left(\overline{f_{xx} f_{yy}}\right)_{ij} \\ & + 2 \sum_{i,j\in B} \left(\hat{\rho}_4(\bar{0})\right)_{(k+i)(l+j)} \left(\overline{f_{xx} f_{xy}}\right)_{ij} + 2 \sum_{i,j\in B} \left(\hat{\rho}_5(\bar{0})\right)_{(k+i)(l+j)} \left(\overline{f_{yy} f_{xy}}\right)_{ij}\end{aligned} \tag{42}$$

with $\bar{\rho}_1(\bar{0})$–$\bar{\rho}_6(\bar{0})$ as:

$$\begin{aligned}\left(\bar{\rho}_1(\bar{0})\right)_{ij} &= \left(\cos^4\varphi', \lambda(\bar{r}' - \bar{r}_{ij})\right)_{\bar{r}} \\ \left(\bar{\rho}_2(\bar{0})\right)_{ij} &= \left(\sin^4\varphi', \lambda(\bar{r}' - \bar{r}_{ij})\right)_{\bar{r}} \\ \left(\bar{\rho}_3(\bar{0})\right)_{ij} &= \left(\sin^2 2\varphi', \lambda(\bar{r}' - \bar{r}_{ij})\right)_{\bar{r}} \\ \left(\bar{\rho}_4(\bar{0})\right)_{ij} &= \left(\cos^2\varphi' \sin 2\varphi', \lambda(\bar{r}' - \bar{r}_{ij})\right)_{\bar{r}} \\ \left(\bar{\rho}_5(\bar{0})\right)_{ij} &= \left(\sin^2\varphi' \sin 2\varphi', \lambda(\bar{r}' - \bar{r}_{ij})\right)_{\bar{r}}\end{aligned} \tag{43}$$

The number of kernels seems to be 5, but this number can be reduced to 2 by rewriting the trigonometric functions above as functions of $\cos 4\varphi$, $\sin 4\varphi$, $\cos 2\varphi$, $\sin 2\varphi$. The filters connected to case 2) and given in the equations (19)-(21) can also be rewritten to be functions of $\cos 2\varphi$ and $\sin 2\varphi$. Hence the two filters become

$$\begin{aligned}\left(\bar{\rho}_1'(\bar{0})\right)_{ij} &= \left(\cos 4\varphi', \lambda(\bar{r}' - \bar{r}_{ij})\right)_{\bar{r}} \\ \left(\bar{\rho}_2'(\bar{0})\right)_{ij} &= \left(\sin 4\varphi', \lambda(\bar{r}' - \bar{r}_{ij})\right)_{\bar{r}}\end{aligned} \tag{44}$$

Here we give the error bounds due to the approximations of $\bar{\rho}_1(\bar{0})$, table 3.4). The truncation error bounds for $\bar{\rho}_2(\bar{0})$ is the same as $\hat{\rho}_1(\bar{0})$ for symmetry reasons.

6) $\left(\frac{\partial^2 f}{\partial \varphi'^2}, \frac{\partial^2 f}{\partial \varphi'^2}\right)_{\bar{r}}$

Like in case 5) we will apply the chain rule to (28) and get:

$$\frac{\partial^2 f}{\partial \varphi'^2} = r'^2 \sin^2 \varphi' \frac{\partial^2 f}{\partial x'^2} + r'^2 \cos^2 \varphi' \frac{\partial^2 f}{\partial y'^2} - r'^2 \sin 2\varphi' \frac{\partial^2 f}{\partial x' \partial y'} \tag{45}$$

This will provide us with:

$$\begin{aligned}
&\left(\frac{\partial^2 f}{\partial \varphi'^2}, \frac{\partial^2 f}{\partial \varphi'^2}\right)_{\bar{r}} = \left(1, \left(\frac{\partial^2 f}{\partial \varphi'^2}\right)^2\right)_{\bar{r}} \\
&= \left(r'^4 \sin^4 \varphi', \left(\frac{\partial^2 f}{\partial x'^2}\right)^2\right)_{\bar{r}} + \left(r'^4 \cos^4 \varphi', \left(\frac{\partial^2 f}{\partial y'^2}\right)^2\right)_{\bar{r}} + \left(r'^4 \sin^2 2\varphi', \left(\frac{\partial^2 f}{\partial x' \partial y'}\right)^2\right)_{\bar{r}} \\
&= +\frac{1}{2}\left(r'^4 \sin^2 2\varphi', \frac{\partial^2 f}{\partial x'^2} \cdot \frac{\partial^2 f}{\partial y'^2}\right)_{\bar{r}} - 2\left(r'^4 \sin^2 \varphi' \sin 2\varphi', \frac{\partial^2 f}{\partial x'^2} \frac{\partial^2 f}{\partial x' \partial y'}\right)_{\bar{r}} \\
&- 2\left(r'^4 \cos^2 \varphi' \sin 2\varphi', \frac{\partial^2 f}{\partial x'^2} \frac{\partial^2 f}{\partial x' \partial y'}\right)_{\bar{r}}
\end{aligned} \tag{46}$$

Then we get

$$\begin{aligned}
\left(\frac{\partial^2 f}{\partial \varphi'^2}, \frac{\partial^2 f}{\partial \varphi'^2}\right)_{\bar{r}} \approx &\sum_{i,j \in B} \left(\hat{v}_1(\bar{0})\right)_{(k+i)(l+j)} \left(\overline{f_{xx}^2}\right)_{ij} + \sum_{i,j \in B} \left(\hat{v}_2(\bar{0})\right)_{(k+i)(l+j)} \left(\overline{f_{yy}^2}\right)_{ij} + \\
&\sum_{i,j \in B} \left(\hat{v}_3(\bar{0})\right)_{(k+i)(l+j)} \left(\overline{f_{xy}^2}\right)_{ij} + \frac{1}{2} \sum_{i,j \in B} \left(\hat{v}_3(\bar{0})\right)_{(k+i)(l+j)} \left(\overline{f_{xx} f_{yy}}\right)_{ij} \\
&- 2 \sum_{i,j \in B} \left(\hat{v}_4(\bar{0})\right)_{(k+i)(l+j)} \left(\overline{f_{xx} f_{xy}}\right)_{ij} - 2 \sum_{i,j \in B} \left(\hat{v}_5(\bar{0})\right)_{(k+i)(l+j)} \left(\overline{f_{yy} f_{xy}}\right)_{ij}
\end{aligned} \tag{47}$$

with

R	R'	σ_{v_3}
6.0	10	0.003
7.0	11	0.003
8.0	11	0.003

R	R'	σ_{v_4}
6.0	14	0.003
7.0	14	0.003
8.0	12	0.001

Table 3.5): The relative errors made by truncating $\bar{v}_3$ and $\bar{v}_4$.

$$
\begin{aligned}
\left(\bar{v}_1(\bar{0})\right)_{ij} &= \left(r'^4 \sin^4\varphi', \lambda(\bar{r}' - \bar{r}_{ij})\right)_{\bar{r}} \\
\left(\bar{v}_2(\bar{0})\right)_{ij} &= \left(r'^4 \cos^4\varphi', \lambda(\bar{r}' - \bar{r}_{ij})\right)_{\bar{r}} \\
\left(\bar{v}_3(\bar{0})\right)_{ij} &= \left(r'^4 \sin^2 2\varphi', \lambda(\bar{r}' - \bar{r}_{ij})\right)_{\bar{r}} \\
\left(\bar{v}_4(\bar{0})\right)_{ij} &= \left(r'^4 \sin^2\varphi' \sin 2\varphi', \lambda(\bar{r}' - \bar{r}_{ij})\right)_{\bar{r}} \\
\left(\bar{v}_5(\bar{0})\right)_{ij} &= \left(r'^4 \cos^2\varphi' \sin 2\varphi', \lambda(\bar{r}' - \bar{r}_{ij})\right)_{\bar{r}}
\end{aligned}
$$

The errors associated with $\bar{v}_2 ... \bar{v}_4$ are given in the table 3.4) and table 3.5).

In the cases 2)-6) the discretized versions of the following pictures were assumed to exist:

1) $\bar{f}_x$, $\bar{f}_y$

2) $\hat{f}_{xx}$, $\hat{f}_{yy}$, $\hat{f}_{xy}$

We propose to evaluate these pictures and store them before computations proposed earlier. One might be tempted to use a reconstructed band limited picture as before to evaluate these partial derivative pictures. But the problem with this is the slow decay of the coefficients for 2-D case. In 1-D cases one can accelerate it by taking derivatives in midpoints, $x = \frac{k}{2}$;

$$
\frac{\partial f}{\partial x} = \sum_i f(x_i) \frac{\pi(x-i)\cos\pi(x-i) - \sin\pi(x-i)}{\pi(x-i)^2} \tag{48}
$$

$$
\frac{\partial f}{\partial x}\Big|_{x=\frac{k}{2}} = \sum_i f(x_i) \frac{(-1)^i}{\pi(k-i+0.5)^2} \tag{49}
$$

which is a quadratic decay. But for 2-D cases one can not evaluate $\frac{\partial f}{\partial x}$ and $\frac{\partial f}{\partial y}$ at the same point with the same decay rate at all directions.

$$\frac{\partial f}{\partial x} = \sum_{ij} f(\bar{r}_{ij}) \frac{\pi(x-i)\cos\pi(x-i) - \sin\pi(x-i)}{\pi(x-i)^2} \frac{\sin\pi(y-j)}{\pi(y-j)^2} \tag{50}$$

$$\frac{\partial f}{\partial x}\Big|_{\substack{x=k \\ y=0}} = \sum_{ij} f(\bar{r}_{ij}) \frac{(-1)^i}{k-i}$$

This would result in a very large mask to give acceptable truncation error. Instead we will adopt schemes offered by numerical methods, [13]. The derivative of a function is computed by means of it's values on a grid according to [14]:

$$\begin{aligned} D_x f_0 &= \mu_x \delta_x \sum_{n=0}^{\infty} (-1)^n \frac{(n!)^2}{(2n+1)!} \delta_x^{2n} f_0 \\ &= \mu_x \delta_x \Big(1 - \frac{\delta_x^2}{6} + \frac{\delta_x^2}{30} - \frac{\delta_x^6}{140} + \frac{\delta_x^8}{630} - \frac{\delta_x^{10}}{2772} + \frac{\delta_x^{12}}{12012} \cdots\Big) f_0 \end{aligned} \tag{51}$$

where

$$\begin{aligned} f_0 &= f(\bar{r}_{kl}) \\ D_x &= \frac{\partial}{\partial x} \\ \delta_x &= \big(E_x^{\frac{1}{2}} - E_x^{\frac{-1}{2}}\big) \\ \mu_x &= \frac{1}{2}\big(E_x^{\frac{1}{2}} - E_x^{\frac{-1}{2}}\big) \end{aligned} \tag{52}$$

Here E_x is the translation operator, which defines the operators δ_x and μ_x:

$$E_x^t f_0 = f(x_k, y_l) \qquad \text{for} \qquad \bar{r}_{kl} = (x_k, y_l).$$

Since (51) contains only even exponents of

$$\delta_x$$

and $\mu_x \delta_x = \frac{1}{2}\big(E_x - E_x^{-1}\big)$ the evaluation corresponding to (51) will only include the values of f at the grid points. This is what we wanted. We approximate $D_x f_0$ by truncating (51):

$$D_x f_0 = \mu_x \delta_x \sum_{n=0}^{N-1} (-1)^n \frac{(n!)^2}{(2n+1)!} \delta_x^{2n} f_0 \tag{53}$$

Both (51) and (53) can be thought of as ordinary scalar products $\bar{\partial}_x^t \bar{f}$ and $\hat{\partial}_x^t \bar{f}$ as before. It should be observed that $\hat{\partial}_x$ is not a simple truncation of $\bar{\partial}_x$. The components of $\bar{\partial}_x$ and $\hat{\partial}_x$ are found by inserting (52) in (51) and (53) and using the binomial expansion. The truncation error of $\bar{\partial}_x$ defined by

$$\bar{\partial}_x = \hat{\partial}_x + \bar{\epsilon}_\partial \tag{54}$$

can be found to yield:

$$\frac{\bar{\epsilon}_\partial}{\|\bar{\partial}_x\|_\infty} \approx \frac{(N!)^2}{(2N+1)!} \tag{55}$$

A similar expansion to (51) exists for $D_x^2 f_0$, [14].

$$\begin{aligned} D_x^2 f_0 = 2 \sum_{n=1}^{\infty} (-1)^{n-1} \frac{[(n-1)!]}{(2n)!} f_0 \\ (\delta_x^2 - \frac{\delta_x^4}{12} + \frac{\delta_x^6}{90} - \frac{\delta_x^8}{560} + \frac{\delta_x^{10}}{3150} - \frac{\delta_x^12}{16632} \ldots) f_0 \end{aligned} \tag{56}$$

Approximation is obtained by truncation of this sum, resulting in a scalar product between two vectors. By using (51) twice we get:

$$D_x D_y f_0 = \mu_x \mu_y \delta_x \delta_y \sum_{m,n} (-1)^{m+n} \frac{m!}{(2m+1)!} \frac{n!}{(2n+1)!} \delta_x^{2m} \delta_x^{2n} f_0 \tag{57}$$

with $m, n \; in \{0, 1, 2 \ldots\}$. Up to now we were only concerned with errors made by replacing a large vector $\bar{\cdot}$ with a smaller vector $\hat{\cdot}$ for individual quantities and did not worry about the composite truncation error made.

For example in

$$\left(\cos^2(\varphi'), (\frac{\partial f}{\partial x'})^2\right)_{\bar{r}} = \bar{\beta}(\bar{r})\overline{f_x^2} \tag{58}$$

we based our truncation error for $\beta(\bar{r})$ on the assumption that we had access to an error free picture $\overline{f_x^2}$. Later (51), we have given an approximation to $\overline{f_x^2}$. How do these two errors influence the final error of (58) originating from truncating two vectors? In the following paragraph we will try to answer this question.

Let us denote the finite dimensional vector space, containing the finite dimensional discretized version of the picture $\bar{f}$ as X. Moreover, let $\bar{g}$ be a transformation from

$$Y = X \otimes X \otimes X \otimes X \tag{59}$$

to X defined as:

$$\bar{g}(\overline{T}_1, \overline{T}_2, \overline{T}_3, \overline{T}_4) = \overline{T}_4 * \left((\overline{T}_3 * \overline{T}_1) \circ (\overline{T}_2 * \overline{T}_1)\right) \tag{60}$$

for

$$\overline{T}_1, \overline{T}_2, \overline{T}_3, \overline{T}_4 \in Y$$

where $*$ is the convolution:

$$\left(\overline{T}_1 * \overline{T}_2\right)_{kl} = \sum_{ij} \left(\overline{T}_1\right)_{(k+i)(l+j)} \left(\overline{T}_2\right)_{ij} \qquad \overline{T}_1, \overline{T}_2 \in X \tag{61}$$

and $\circ$ represents component wise multiplication:

$$\left(\overline{T}_1 \circ \overline{T}_2\right)_{kl} = \left(\overline{T}_1\right)_{kl} \left(\overline{T}_2\right)_{kl} \qquad \overline{T}_1, \overline{T}_2 \in X \tag{62}$$

It is obvious that $\overline{T}_1 * \overline{T}_2 \in X$ and $\overline{T}_1 \circ \overline{T}_2 \in X$, if the dimension of X is sufficiently larger than $\overline{T}_1$ and $\overline{T}_2$'s. We adopt $\|.\|_\infty$ as norm for X and Y. All key quantities can now be expressed by sums of $\bar{g}$, for example

$$\left(\cos^2(\varphi'),(\frac{\partial f}{\partial x'})^2\right)_{\bar{r}} = \bar{\beta}(\bar{0}) * \left((\bar{\partial}_x * \bar{f}) \circ (\bar{\partial}_x * \bar{f})\right) \tag{63}$$

which is obtained through (15), (19), (54) as we have $\overline{T}_1 = \bar{f}$, $\overline{T}_3 = \overline{T}_4 = \bar{\partial}_x$, $\overline{T}_4 = \bar{\beta}(\bar{0})$. That $\bar{g}$ is continuous in $\overline{T} = \left(\overline{T}_1, \overline{T}_2, \overline{T}_3, \overline{T}_4\right) \in Y$ is obvious, because $\bar{g}$ can be expressed as ordinary finite sums and products of real variables. Thus

$$\|\bar{g}(\overline{T} + \bar{h}) - \bar{g}(\overline{T})\|_\infty \leq \epsilon \tag{64}$$

for $\overline{T}, \bar{h} \in Y$, where $\epsilon \to \infty$ as $\|\bar{h}\|_\infty \to 0$. This leads to that there exists a δ for any ϵ such that:

$$\frac{\|\bar{g}(\overline{T} + \bar{h}) - \bar{g}(\overline{T})\|_\infty}{\|\bar{g}(\overline{T})\|_\infty} \leq \epsilon$$

as soon as $\|\bar{h}\|_\infty \leq \delta$ and $\bar{g}(\overline{T})$ are non vanishing. This simply means that $\bar{g}(\overline{T})$ can be approximated by $\bar{g}(\overline{T} + \bar{h})$ as well as desired by decreasing $\|\bar{h}\|_\infty$. In the following we will show that the round off errors due to word length limitation in picture representation will not allow us to do this as much as we wish.

We will set $\bar{h} = (\bar{h}_1, \bar{h}_2, \bar{h}_3, \bar{h}_4)$ since $\bar{h} \in Y$ and try to approximate by that the variation in $\bar{g}(\overline{T})$ as:

$$\bar{g}(\overline{T} + \bar{h}) - \bar{g}(\overline{T}) = \mathcal{L}(\bar{h}) + \alpha(\overline{T}, \bar{h}) \tag{65}$$

where $\mathcal{L}$ is a linear operator and $\frac{\|\bar{\alpha}(\overline{T},\bar{h})\|_\infty}{\|\bar{h}\|_\infty} \to 0$ as $\|\bar{h}\|_\infty \to 0$. This would allow us to see $\bar{g}(\overline{T} + \bar{h}) - \bar{g}(\overline{T})$ as a linear variation with respect to $\bar{h}$:

$$\begin{aligned}\frac{\bar{g}(\overline{T} + t\bar{h}) - \bar{g}(\overline{T})}{t} = \frac{1}{t}(\overline{T}_4 + t\bar{h}_4) * \left(((\overline{T}_3 + t\bar{h}_3) * (\overline{T}_1 + t\bar{h}_1)) \circ ((\overline{T}_2 + t\bar{h}_2) * (\overline{T}_1 + t\bar{h}_1))\right) \\ - \overline{T}_4 * \left((\overline{T}_3 * \overline{T}_1) \circ (\overline{T}_2 * \overline{T}_1)\right)\end{aligned} \tag{66}$$

This can be shown to be equal to

$\mu_x\delta_x f_0$	$\mu_x\delta_x^3 f_0$	$\mu_x\delta_x^5 f_0$	$\mu_x\delta_x^7 f_0$
$0.5U$	$1.5U$	$5U$	$17.5U$

Table 3.6): The round off error made by truncating $D_x f_0$ at various levels.

$$\begin{aligned}&\overline{T}_4 * \left((\overline{T}_3 * \overline{T}_1) \circ (\overline{T}_2 * \bar{h}_1)\right) + \overline{T}_4 * \left((\overline{T}_3 * \overline{T}_1) \circ (\bar{h}_2 * \overline{T}_1)\right) \\ &+ \overline{T}_4 * \left((\overline{T}_3 * \bar{h}_1) \circ (\overline{T}_2 * \overline{T}_1)\right) + \overline{T}_4 * \left((\bar{h}_3 * \overline{T}_1) \circ (\overline{T}_2 * \overline{T}_1)\right) \\ &+ \bar{h}_4 * \left((\overline{T}_3 * \overline{T}_1) \circ (\overline{T}_2 * \overline{T}_1)\right) + \bar{\alpha}(\overline{T}, t\bar{h})\end{aligned} \tag{67}$$

after a straight forward usage of the additivity property of $*$ and $\circ$:

$$\begin{aligned}\overline{T}_1 * (\overline{T}_2 + \overline{T}_3) &= \overline{T}_1 * \overline{T}_2 + \overline{T}_1 * \overline{T}_3 \\ \overline{T}_1 \circ (\overline{T}_2 + \overline{T}_3) &= \overline{T}_1 \circ \overline{T}_2 + \overline{T}_1 \circ \overline{T}_3\end{aligned} \tag{68}$$

$\bar{\alpha}(\overline{T}, t\bar{h})$ is a function for which

$$\lim_{t \to 0} \frac{\bar{\alpha}(\overline{T}, t\bar{h})}{t} = constant \tag{69}$$

yields. The operator given in (67) is linear in $\bar{h}$ because $*$ and $\circ$ have additivity property according to (68). Since only $*$ and $\circ$ are involved in (67), it is also continuous leading to the fact that $\bar{g}(\overline{T})$ is differentiable in $\bar{T}$ and the linear operator in (67) becomes unique, [4], and can be identified as $\mathcal{L}$ in (65). In all key quantity evaluations $\overline{T}_1$ is the picture. We see that errors in picture values, $\bar{h}_1$, caused by digitization appears twice in (67). Only this fact alone suggests not to be too diligent in trying to decrease the truncation errors $\bar{h}_2$, $\bar{h}_3$, $\bar{h}_4$ too much. The other argument for not being too diligent in decreasing the truncation errors $\|\bar{h}_2\|_\infty$ and $\|\bar{h}_3\|_\infty$ is that these in almost all key quantity evaluations, correspond to truncation errors made in connection with partial derivative approximations. Decreasing $\|\bar{h}_2\|_\infty$ and $\|\bar{h}_3\|_\infty$ means that one takes more and more terms, for example in (51). If the smallest positive number representable in the data structure of the picture is U, then the discretization error is 1/2 U. The approximation of $\frac{\partial f}{\partial x}\big|_{\bar{r}_{kl}}$ yields the round off error bound:

$$R_{XF} = \frac{u}{2} \sum_i \left|(\hat{\partial}_x)_i\right| \tag{70}.$$

This sum is given below for the approximations done by truncating at the following terms.

The table shows that R_{XF} increases with decreased truncation error. Usually it does not pay to take more than a few terms to the sum, before R_{XF} becomes the dominating error source. In fact, if any of the approximations to $\overline{T}_2$, $\overline{T}_3$, $\overline{T}_4$ has diverging absolute sums of their components, we will have this phenomenon. As a conclusion to this chapter we should not expect to decrease the total amount of error to arbitrarily low levels by decreasing the truncation error, because this has the effect of not only increasing the size of masks, but also directly increasing the round off error, due to inaccurate picture representation. To have a qualitative comprehension of how different types of errors effects the total error (67) can be used. This tells us that for small errors in approximation of $\bar{T}$, all errors originating from different vector approximations affect the total error linearly and separately.

CHAPTER 4
LINEAR SYMMETRY MODELLING

In this chapter we will describe local neighbourhoods in terms of linear symmetry. Even though a quite direct application of this is to detect lines and edges, our approach will not be to model these properties directly. As it was announced earlier in chapter 2, we will follow the ideas developed there.

The characteristic property of lines and edges is that the locus of their iso gray values are parallel lines in cartesian coordinates. The natural complete basis functions on a rectangle with this property are sine and cosine functions. Here we will denote this rectangle by Ω. The completition of $C^2(\Omega)$ becomes a Hilbert space with the scalar product:

$$(f,g) = \frac{1}{|\Omega|}\int_{\Omega} f^*(\bar{r})g(\bar{r})d\Omega \tag{1}$$

where

$$|\Omega| = \int_{\Omega} d\Omega.$$

The functions $\{\Psi_{mn}\}_{m,n\in Z}$

$$\Psi_{mn}(\bar{r}) = e^{i(m\omega_x x + n\omega_y y)} \tag{2}$$

where $\omega_x = \frac{2\pi}{L_x}$ and $\omega_y = \frac{2\pi}{L_y}$ with L_x and L_y being the side length of the rectangle in horizontal respectively vertical direction, x and y are local cartesian coordinates. Actually these functions are orthonormal and dense in $\mathcal{L}^2(\Omega)$.

Consider a square shaped neighbourhood with sides L. A function, f, which is assumed to be in $C^2(\Omega)$, can be expanded evenly as in chapter 2.

For this purpose we define f outside of the square, in which it is well defined as:

$$f(-x,-y) = f(x,y) \qquad (x,y) \in [0,L] \otimes [0,L]$$

Then we impose periodicity in x and y directions with L respectively $2L$:

$$f(x+L,y) = f(x,y)$$
$$f(x,y+2L) = f(x,y)$$

Thus we have extended f's basic rectangle from $[0,L] \otimes [0,L]$ to $[0,L] \otimes [0,2L]$. Call the latter Ω. Using (1) and (2) together with (3) we find

$$f(\bar{r}) = \sum_{m,n \in Z} c_{mn} \Psi_{mn}(\bar{r}) \tag{4}$$

with

$$\begin{aligned} c_{mn} &= (f, \Psi_{mn}) \\ &= \frac{1}{2L^2} \int_{\Omega} f(\bar{r}) \Psi_{mn}(\bar{r}) d\Omega \end{aligned} \tag{5}$$

Using the fact that f is even we arrive

$$f = \sum_{m,n \in H} a_{mn} \phi_{mn} \tag{6}$$

with

$$\phi_{mn} = \frac{cos(m\omega_x x + n\omega_y y)}{\|cos(m\omega_x x + n\omega_y y)\|} \qquad , \omega_x = \frac{2\pi}{L}, \quad \omega_y = \frac{\pi}{L} \tag{7}$$

$$a_{mn} = (f, \phi_{mn}) = \frac{1}{2L^2} \int_{\Omega} f \phi_{mn} d\Omega \tag{8}$$

The functions $\{\phi_{mn}\}_{m,n \in H}$ are orthonormal. This means that every function $f(x,y) \in C^2(\Omega)$ can be approximated arbitrarily well. by a weighted sum of trigonometric functions, ϕ_{mn}, everyone of which possessing a definite direction. That is every function $f(x,y) \in C^2(\Omega)$ will have a unique portrait (spectrum) in H. We will try to conclude whether there is some sort of concentration to certain areas of H as in chapter 2.

POINT CONCENTRATION

We approximate the location of point concentration as in the circular symmetry case:

$$m_d^2 = \sum_{m,n \in H} \frac{a_{mn}^2}{A^2} m^2 \tag{9}$$

where

$$A^2 = \sum_{m,n \in H} a_{mn}^2$$

These can be computed through the Parseval relation with the given scalar product:

$$\begin{aligned} A^2 &= \|f\|^2 \\ m_d^2 &= \frac{\|D_x f\|^2}{A^2 \omega_x^2} \end{aligned} \tag{10}$$

The confidence measure looks also identical as before

$$\begin{aligned} C_{\Omega m}^2 &= \sum_{m,n \in H} \frac{a_{mn}^2}{A^2} (m^2 - m_d^2)^2 \\ &= \frac{\|D_x^2 f\|^2}{A^2 \omega_x^4} - m_d^4 \end{aligned} \tag{11}$$

The only difference is the scalar product. Without further motivation we state:

$$\begin{aligned} n_d^2 &= \sum_{m,n \in H} \frac{a_{mn}^2}{A^2} n^2 = \frac{\|D_y f\|^2}{A^2 \omega_y^2} \\ C_{\Omega n}^2 &= \sum_{m,n \in H} \frac{a_{mn}^2}{A^2} (n^2 - n_d^2)^2 \\ &= \frac{\|D_y^2 f\|^2}{A^2 \omega_y^4} - n_d^4 \end{aligned} \tag{12}$$

The decision concerning in which half plane of H the concentration is, is determined by a sign variable which will be determined by the sign of the weighted mixed product:

$$p = \sum_{m,n \in H} \frac{a_{mn}^2}{A^2} mn \tag{13}$$

which we will come back to later.

LINE CONCENTRATION

The line concentration in the H plane simply means existence of a definite direction in the function f, which is our local neighbourhood in the picture. As in [5], this information together with a confidence parameter should be an alternative method to extract lines and edges efficiently. However, the main purpose is not to detect lines and edges as such but to extract a very well defined property of lines and edges, that is their orientation. A neighbourhood with iso-gray values having a definite direction will give rise to line concentration in H plane. The direction, θ, minimizing the degradation:

$$C_{\Omega\theta} \stackrel{\triangle}{=} \sum_{m,n \in H} (n\sin(\theta) - m\cos(\theta))^2 \frac{a_{mn}^2}{A^2} \tag{14}$$

is given by

$$\theta_d = \frac{1}{2}\tan^{-1}(n_d^2 - m_d^2, 2p). \tag{15}$$

which is the least square fitting of a line through origin in the transform plane. Since orientation of a line structure is unaltered upon 180° rotation of the neighbourhood it is possible to define orientation as twice the argument of the directional vector. This leads us to a continuous representation of orientation by the argument of a vector [5] & [8]'s algorithm provides this vector naturally. including the factor two, guaranteeing the continuity of the argument. It is interesting to note that the complex number (vector)

$$z = (n_d^2 - m_d^2 + i2p)\frac{1}{\sqrt{(n_d^2 - m_d^2)^2 + 4p^2}} \tag{16}$$

also possesses this property:

$$\begin{aligned} arg(z) &= 2\theta_d \\ |z| &= 1 \end{aligned} \tag{17}$$

The estimated θ_d, put in (14), provides the confidence measure:

$$C_{\Omega\theta} = \frac{1}{2}\left(n_d^2 + m_d^2 - \sqrt{(n_d^2 - m_d^2)^2 + 4p^2}\right). \tag{18}$$

Thus, if one uses the GOP representation, the complex number representing local orientation becomes

$$zg(C_{\Omega\theta}) \tag{19}$$

where g is any suitable decreasing real function of $C_{\Omega\theta}$ scaled to fit the gray value depth. The argument of a vector in GOP representation stands for class representation and magnitude for class membership certainty.

CHAPTER 5
DESIGNING FILTERS FOR LINEAR SYMMETRY DETECTION

When we considered the local neighbourhoods as the even expansions in

$$\{\cos(mw_x x + nw_y y\}_{m,n\in H}$$

we had concluded that we needed (f,f), $(\frac{\partial f}{\partial x},\frac{\partial f}{\partial x})$, $(\frac{\partial f}{\partial y},\frac{\partial f}{\partial y})$, $(\frac{\partial f}{\partial x},\frac{\partial f}{\partial y})$, $(\frac{\partial^2 f}{\partial x^2},\frac{\partial^2 f}{\partial x^2})$, $(\frac{\partial^2 f}{\partial y^2},\frac{\partial^2 f}{\partial y^2})$ for the determination of point and line concentration properties in the spectra. The image represented by f was an even expansion of the local neighbourhood and Ω was $[0,L]\otimes[0,2L]$. As in chapter 3) it can be shown that all key quantities mentioned above can be calculated without even expansion of the local image. Then the scalar product definition will be:

$$(f,g)=\frac{1}{|\Omega|}\int_{\Omega} f^*(\bar{r})g(\bar{r})d\Omega \tag{1}$$

with Ω being $[0,L]\otimes[0,L]$.

Assuming that f is bandlimited and oversampled at least twice, $\{f(\bar{r}_{ij})\}_{m,n\in B}$, then f is retrievable from it's samples through

$$f(\bar{r})=\sum_{i,j\in B} f(\bar{r}_{ij})\lambda(\bar{r}-\bar{r}_{ij}) \tag{2}.$$

This can be inserted in any of the scalar products above and we end up with a convolution by a simple filter, $\bar{\ell}$, where coefficients are given by

$$\left(\bar{\ell}(\bar{r})\right)_{ij}\stackrel{\triangle}{=}\left(1,\lambda(\bar{r}'-\bar{r}_{ij})\right)_{\bar{r}} \tag{3}$$

where the index, $\bar{r}$, of the scalar product symbolizes the examined point. To see this we carry out the calculations only for $\left(f,f\right)$.

$$(f,f)=\sum_{i,j\in B} f^2(\bar{r}_{ij})(1,\lambda(\bar{r}'-\bar{r}_{ij})) \tag{4}$$

L	L'	σ_ℓ
6.0	11	0.003
7.0	11	0.003
8.0	11	0.003

Table 5.1): The relative errors made by truncating $\bar{\ell}$.

Since partial derivatives with respect to cartesian coordinates are unchanged by shifting the examined point we get

$$\begin{aligned}
(f,f) &= \overline{f^2} * \bar{\ell} \\
(\frac{\partial f}{\partial x}, \frac{\partial f}{\partial x}) &= \overline{f_x^2} * \bar{\ell} \\
(\frac{\partial f}{\partial y}, \frac{\partial f}{\partial y}) &= \overline{f_y^2} * \bar{\ell} \\
(\frac{\partial f}{\partial x}, \frac{\partial f}{\partial y}) &= \overline{f_x f_y} * \bar{\ell} \\
(\frac{\partial^2 f}{\partial x^2}, \frac{\partial^2 f}{\partial x^2}) &= \overline{f_{xx}^2} * \bar{\ell} \\
(\frac{\partial^2 f}{\partial y^2}, \frac{\partial^2 f}{\partial y^2}) &= \overline{f_{yy}^2} * \bar{\ell}.
\end{aligned} \tag{5}$$

As before we approximate $\bar{\ell}$ by truncating it. We propose a square truncation,

$$(\hat{\ell})_{ij} = \begin{cases} (\bar{\ell})_{ij}, & \text{if } \bar{r}_{ij} \in \Omega'; \\ 0, & \text{otherwise.} \end{cases} \tag{9}$$

such that the largest component left out divided by the largest component of $\hat{\ell}$, call this ratio σ_ℓ, is small enough. Ω', is the truncation square with side length L'. In table 5.1) we give L' and σ_ℓ for some L's.

CONCLUSION

In the previous chapters we have defined two types of symmetries. The behaviour of the spectrum was crucial for the feature parameters presented. The local neighbourhood was well defined by it's boundaries and the image was expanded locally by means of two basis function sets. As a result of these Fourier series expansions, the pattern of the periodic repetition of the neighbourhood influences the behaviour of the spectra.

To illuminate some effects of this phenomenon, let us consider the linear symmetry case. An edge found in a local neighbourhood has a definite orientation when it is not periodized. However, Fourier series expansion will not give a perfect line concentration in the spectrum due to periodization. Instead we get a concentration around a line because the stated approach in the previous chapter will take all edges into account, possibly including some eventuel extra edges obtained by periodization. What we get from the line concentration algorithm is the least square orientation fitted to this periodized neighbourhood.

We get a perfect line concentration in the spectrum, if the neighbourhood consists of a function whose repetition in the vertical and horizontal directions gives rise to a function with the linear symmetry property. That is, the iso gray values of the extended function are parallel lines.

The frequency (point concentration) and the orientation (line concentration) properties of a local neighbourhood are proposed to be measured in the spectral domain. These properties are easily defined in this domain. It is noted that some neighbourhoods may lack the orientation peoperty, that is, a line concentration in the spectrum in the least squares sense is not observable. For such neighbourhoods any orientation is equally dominating. It is considered very important to give a confidence measure for the extracted features, since the measured properties are more reliable for some neighbourhoods compared to others. It is shown that the variance from a point respectively a line concentration works for this purpose.

The feature extractions proposed are all carried out in the spatial domain thanks to the Parseval relation. Moreover, they are "second level" operations, since they are carried out on the partial derivative pictures and not on the original picture only. This is intuitively appealing since the investigated properties are direct consequences of the gray value variations of the neighbourhoods.

In the point concentration case the DC–level contributes to the mean-value of the location

of a possible point concentration. In most cases, we deal with non-negative digitized inputs. This has the consequence in the spectrum that the DC–energy becomes the dominating energy and the zero frequency is obtained from the majority of the neighbourhoods as a result of the point concentration investigation. The DC–level effects can be removed easily by subtracting the DC–energy from the total energy of the neighbourhood:

$$A^2 \triangleq (f, f) - (1, f)^2.$$

As an alternative to this subtraction one can use a locally high pass filtered version of the picture. The method remains unchanged in principle. Only the input signal is modified.

REFERENCES

[1] Max Knoll, Johann Kugler, Joseph Eichmeier and Oskar Höfer: "Note on the Spectroscopy of Subjective Light Patterns." Journal of Analytical psychology, No 7, 1962.

[2] Per Lövsund: "Biological Effects of Alternating Magnetic Fields with Special Reference to the Visual System." Dissertation No 47, 1980, Linköping Studies in Science and Technology, Linköping University, Sweden.

[3] W. Rudin: "Real and Complex Analysis." McGraw–Hill, New York, 1969.

[4] A. Wouk: "A course of applied functional analysis." Wiley, New York, 1979.

[5] G.H. Granlund: "In Search of a General Picture Processing Operator." Computer Graphics and Image Processing 8, 155–173 (1978).

[6] G.H. Granlund: "Hierarchical Image Processing." Proceedings of SPIE Technical conference, Geneva, April 18–27, 1983.

[7] I.L. Meriam: "Statics." John Wiley & Sons, New York, 1980.

[8] H. Knutsson: "Filtering and reconstruction in image processing." Dissertation No. 88, 1982, Linköpings Studies in Science and Technology, Linköping University, Sweden.

[9] H.E. Knutsson, R. Wilson and G.H. Granlund: "Anisotropic Nonstationary Image Estimation and It's Applications: Part I–Restoration of Noisy Images." IEEE Transactions on Communications, Vol. Com–31, No.3, March 1983.

[10] Robert A. Hummel: "Feature Detection Using Basis Functions." Computer Graphics and Image Processing 9, 1979.

[11] P.E. Danielsson: "Rotation invariant linear operators with directional response." Proceedings of 5'th international conference on pattern recognition, December 1980.

[12] R. Lenz: "Optimal filtering." Linköping university, Internal Report of the Department of Electrical Engineering, 1985.

[13] G. Dahlquist, Å. Björk: "Numerical Methods." Prentice Hall, Englewood Cliffs, N.J., 1974.

[14] C.E. Fröberg: "Numerical Mathematics." Philadelphia, Addison Wesl. 1985.

[15] A. Papoulis: "Signal Analysis." McGraw–Hill, Int. Stud. Ed., 1977.